catalysts

MDPI

Review

g-C_3N_4-Based Direct Z-Scheme Photocatalysts for Environmental Applications

Javier Fernández-Catalá [1,2,*], Rossella Greco [2], Miriam Navlani-García [1], Wei Cao [2], Ángel Berenguer-Murcia [1] and Diego Cazorla-Amorós [1]

[1] Inorganic Chemistry Department, Materials Science Institute, University of Alicante, Ap. 99, 03080 Alicante, Spain
[2] Nano and Molecular Systems Research Unit, University of Oulu, 90014 Oulu, Finland
* Correspondence: j.fernandezcatala@ua.es

Abstract: Photocatalysis represents a promising technology that might alleviate the current environmental crisis. One of the most representative photocatalysts is graphitic carbon nitride (g-C_3N_4) due to its stability, cost-effectiveness, facile synthesis procedure, and absorption properties in visible light. Nevertheless, pristine g-C_3N_4 still exhibits low photoactivity due to the rapid recombination of photo-induced electron-hole (e^--h^+) pairs. To solve this drawback, Z-scheme photocatalysts based on g-C_3N_4 are superior alternatives since these systems present the same band configuration but follow a different charge carrier recombination mechanism. To contextualize the topic, the main drawbacks of using g-C_3N_4 as a photocatalyst in environmental applications are mentioned in this review. Then, the basic concepts of the Z-scheme and the synthesis and characterization of the Z-scheme based on g-C_3N_4 are addressed to obtain novel systems with suitable photocatalytic activity in environmental applications (pollutant abatement, H_2 production, and CO_2 reduction). Focusing on the applications of the Z-scheme based on g-C_3N_4, the most representative examples of these systems are referred to, analyzed, and commented on in the main text. To conclude this review, an outlook of the future challenges and prospects of g-C_3N_4-based Z-scheme photocatalysts is addressed.

Keywords: direct Z-scheme photocatalyst; g-C_3N_4; pollutant abatement; H_2 production; CO_2 reduction

Citation: Fernández-Catalá, J.; Greco, R.; Navlani-García, M.; Cao, W.; Berenguer-Murcia, Á.; Cazorla-Amorós, D. g-C_3N_4-Based Direct Z-Scheme Photocatalysts for Environmental Applications. *Catalysts* **2022**, *12*, 1137. https://doi.org/10.3390/catal12101137

Academic Editor: Hideyuki Katsumata

Received: 29 August 2022
Accepted: 22 September 2022
Published: 28 September 2022

1. Introduction

Environmental protection and energy generation are two of the great challenges that mankind is presently facing, since they have a large negative impact on our society, affecting, among others, air pollution, climate change, water pollution, thermal pollution, and solid waste disposal [1–3]. Such problems have been caused by rapid industrialization, uncontrolled environmental pollution, and current energy scenario based on fossil fuels [4]. Aiming to solve these issues, current policymakers are passing regulations to reach full environmental sustainability and avoid a prolonged energy crisis and environmental deterioration. One interesting approach to solve this issue is to replace the use of carbon-based energy with solar energy [5,6]. Indeed, solar energy is a green, inexhaustible, and clean resource [6,7]. Another essential approach to achieve the sustainability of our planet is the degradation of pollutants to less toxic products and the reduction of CO_2 to obtain value-added products, which can be achieved under the irradiation of solar light [8,9].

Photocatalysis represents a promising technology that might alleviate the current environmental crisis [10]. Semiconductor photocatalysts may generate H_2 by water splitting, degrade organic pollutants, reduce CO_2 into high value-added products, etc. using solar energy. Moreover, heterogeneous photocatalysis can be performed under very mild conditions (room temperature and atmospheric pressure) [11,12]. Although photocatalytic technology presents relevant characteristics, such as being clean, safe, and renewable, it is still far from commercial implementation, especially in solar-to-fuel conversion [13,14].

Titanium dioxide (TiO_2) has been widely studied in the field of solar energy conversion after the pioneering work reported by Fujishima and Honda in 1972 based on photoelectrochemical water splitting on a TiO_2 electrode [15]. Furthermore, this semiconductor has received great interest from the scientific community for its use in pollutant abatement due to its advantages, e.g., low price, high durability, and abundance [16]. To understand the relevance of photocatalysis, it is important to briefly describe the reaction mechanism [17]. Initially, a photon with energy equal to or greater than the energy band gap (Eg) of the semiconductor is absorbed by the semiconductor. Then, a photoexcited electron (e^-) is promoted from the valence band (VB) to the conduction band (CB). This effect leads to the formation of a hole (h^+) in the VB and, consequentially, to the generation of an electron-hole pair (e^--h^+). The produced e^- and h^+ can recombine on the surface or within the photocatalyst rapidly and thus decrease the photocatalytic activity or they can also migrate to the surface of the semiconductor and initiate the redox reaction(s) with the species adsorbed on the surface of the photocatalyst. The generated holes can induce oxidation processes, which occurs in organic molecules abatement, and the electrons can promote reduction processes such as hydrogen evolution in water splitting and CO_2 reduction. To develop efficient photocatalysts, light absorption is an essential step in the manufacture of the material [18]. Pristine TiO_2 is active only under UV light with a wavelength below 387 nm due to its wide bandgap (3.2 eV). This fact is the main drawback of TiO_2 since solar energy is mainly concentrated (between 95 and 97%) in the IR and visible light regions [16]. Consequently, the exploration of visible-light-responsive photocatalysts with high efficiency is a highly interesting topic for the scientific community [19,20].

Graphitic carbon nitride (g-C_3N_4) is a very promising material due to its potential application in photocatalytic pollutant degradation, photocatalytic H_2 production, and CO_2 reduction. Its bandgap of 2.7 eV makes it a good candidate as a visible-light-responsive photocatalyst. In addition, g-C_3N_4 presents a unique electronic band structure, low cost, and easy preparation, allowing it to be a possible alternative to TiO_2 in solar energy applications [21,22]. However, pristine g-C_3N_4 still exhibits low photoactivity in several applications such as water splitting and CO_2 reduction due to the rapid recombination of photo-induced e^--h^+ pairs [23]. In recent years, several strategies have been developed by the scientific community to improve the photocatalytic efficiency of g-C_3N_4, i.e., morphological control, doping elements, deposition of noble metals, and construction of heterojunctions [24,25].

The latest advancements on g-C_3N_4-related photocatalytic systems are based on g-C_3N_4-based heterostructures due to the effective separation of photogenerated e^--h^+ pairs [26,27]. Traditional heterojunctions are categorized into type-I, type-II, and type-III, as shown in Figure 1. A different pathway of the traditional type-II is the Z-scheme family (Z-schemes and S-schemes) [28,29], as shown in Figure 1 [30,31]. Since the present review is focused on direct Z-scheme heterojunctions, only type II heterojunctions will be described, as shown in Figure 1b. Type II heterojunction formation using g-C_3N_4 is a noteworthy method used to increase the photocatalytic efficiency by suppressing the recombination of charge carriers [24]. However, type II heterostructures limit the oxidation and reduction efficiency of the heterojunction material from the parent materials [27]. To solve this drawback, the synthesis and study of Z-scheme photocatalysts may be a good compromise since Z-scheme-based photocatalysts present the same band configuration but follow a different charge carrier recombination mechanism. Thus, in the Z-scheme, the strongest reduction and oxidation potentials of each semiconductor are preserved similarly to what happens in a natural process such as photosynthesis [32,33].

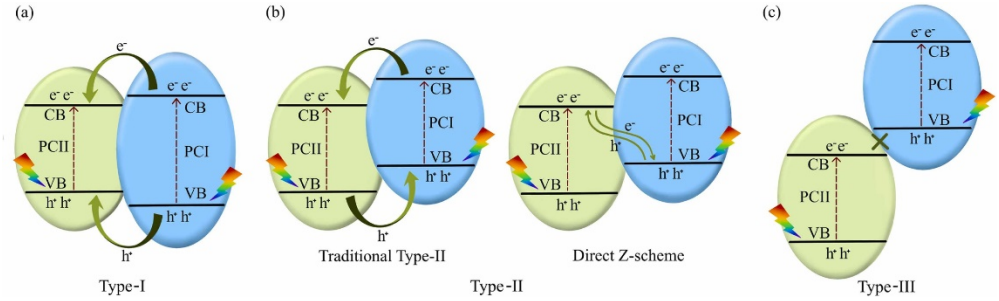

Figure 1. Different types of heterostructures: (**a**) type-I, (**b**) type-II, and (**c**) type-III heterojunctions. Reproduced from [30]. Copyright 2022, Elsevier.

There are two types of Z-scheme semiconductor heterojunctions [34,35]. The first one is the indirect Z-scheme (redox-mediated and all solid state), where the transport route of photogenerated charge carriers is not achieved directly but by the addition of an electron mediator. The second type is the direct Z-scheme, which consists of two semiconductors in close contact, eliminating the demand for an electron mediator. These novel direct Z-scheme photocatalysts have attracted the attention of the scientific community, increasing the use of these photocatalysts. Indeed, the absence of mediators eliminates the backward reaction and light-shielding effects [36,37]. The layered structure of *g*-C_3N_4 is a suitable building block for Z-scheme photocatalyst construction due to the possible high surface area, provided that a layered material is obtained, and its ability to perform photocatalytic reduction reactions (water splitting and CO_2 reduction), making it possible to couple *g*-C_3N_4 with a wide range of oxidation-type photocatalysts to fabricate Z-scheme photocatalysts [21,38,39]. This fact has boosted the study of Z-scheme photocatalysts based on *g*-C_3N_4 for their use in environmental applications, as evidenced by the increase in the number of scientific publications on this topic during the last decade (Figure 2). Therefore, it becomes timely to carry out a bibliographic review in which the most relevant works of direct Z-scheme photocatalysts based on *g*-C_3N_4 and their environmental applications are compiled and summarized.

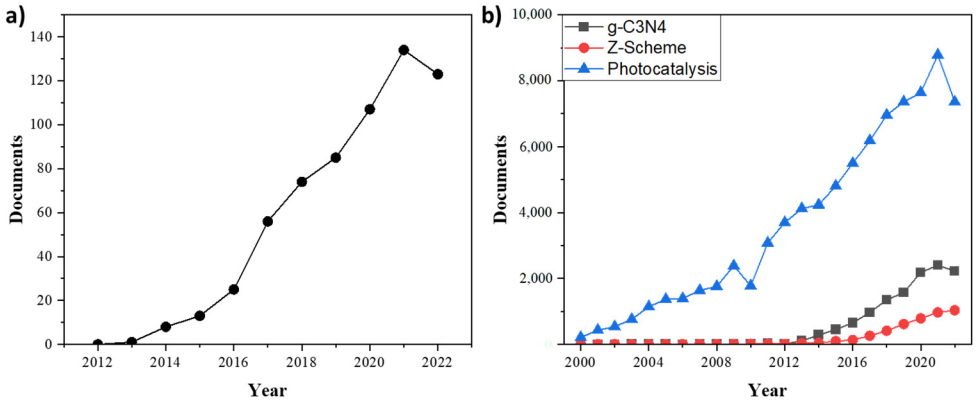

Figure 2. (**a**) Number of publications per year on *g*-C_3N_4-based Z-scheme photocatalysts (source: Scopus; date: 17 July 2022; keywords: "*g*-C_3N_4"; "Z-scheme"; "photocatalysis"). (**b**) Number of publications per year on individual keywords: *g*-C_3N_4-based (black-line) Z-scheme (red-line) and photocatalysis (blue-line) (source: Scopus; date: 8 September 2022).

In this review, we will briefly describe pristine *g*-C_3N_4, although it still exhibits low photoactivity in several applications such as water splitting and CO_2 reduction due to the rapid recombination of photo-induced e^--h^+ pair. Then, a new alternative to improve the photocatalytic activity of *g*-C_3N_4 based on the design of novel Z-schemes will be widely described. Although Z-schemes are applied in relevant photocatalytic reactions, such as environmental applications [34,40], energetic applications [40], transformation of

organic compounds to added-value products [41–43], and photocatalytic biorefineries [44], among others, this review will cover most relevant works on *g*-C_3N_4-based Z-scheme photocatalysts and their use in environmental applications such as pollutant abatement and CO_2 reduction due to the high impact in our society, as was mentioned previously. In addition, energy aspects, e.g., water splitting, are also briefly reviewed.

2. Pristine *g*-C_3N_4

Graphitic carbon nitride is a stable polymeric and layered semiconductor formed by the polymerization of abundant nitrogen-containing precursors, such as melamine or urea [45,46]. The first report about *g*-C_3N_4 was written in the 1830s by Berzelius and Liebig [47]. Since then, many research studies have been carried out to investigate the structure of this material and to develop different synthetic routes [45]. The structure of *g*-C_3N_4 is based on triazine or heptazine units polymerized in a layered structure (Figure 3a) [48,49]. In the last decades, *g*-C_3N_4 has been presented as a promising material for its use in several applications such as sensors, energy storage, and photovoltaic cells, among others, since it presents facile, low-cost, and environmentally friendly preparation methods with promising stability and good physicochemical properties [45,50]. Focusing on the application of this review, *g*-C_3N_4 is a good candidate as a photocatalyst because it is a visible-light-active photocatalyst with a bandgap of ~2.7 eV (~460 nm) [51,52]. In contrast to other semiconductors, *g*-C_3N_4 does not contain metal ions, which may be leached into the ecosystem and cause unfavorable impacts therein. Instead, it is composed of Earth-abundant carbon and nitrogen elements and can be easily synthesized using nitrogen-rich organic precursors by various methods. The obtained *g*-C_3N_4 is endowed with desirable electronic structures and unique morphologies, and high thermal stability up to 600 °C in air [46].

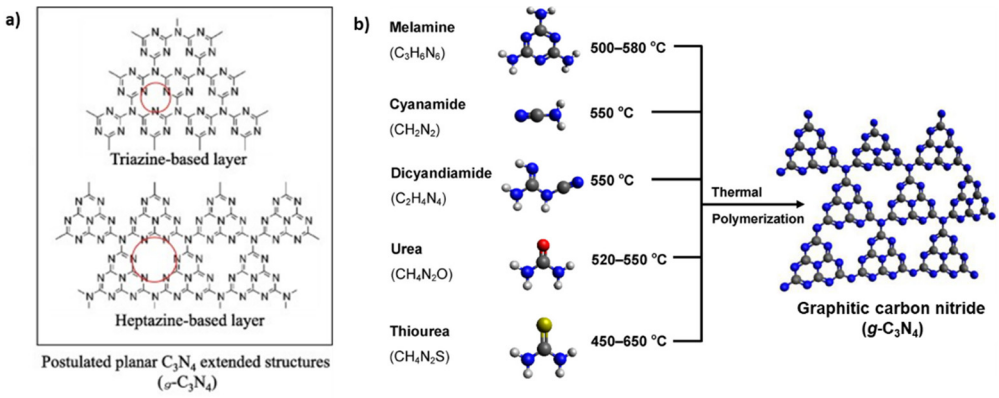

Figure 3. (**a**) Structure of graphitic carbon nitride *g*-C_3N_4. Reproduced from [46]. Copyright 2019, Elsevier. (**b**) Schematic diagram of *g*-C_3N_4 synthesis by thermal polymerization from various precursors (thiourea, melamine, cyanamides, dicyanamide, and urea). Reproduced from [47]. Copyright 2016, ACS Publications.

Nowadays, there are several innovative and relevant synthesis methods of *g*-C_3N_4, that may be classified as solvothermal, chemical vapor deposition (CVD), plasma sputtering reaction deposition, and polycondensation [21,53]. Among them, thermal polycondensation is the most attractive method due to its simplicity and low cost. Nitrogen-rich small molecules can polymerize into *g*-C_3N_4 following a calcination process at 450–650 °C (Figure 3b) [54]. The choice of the precursor exhibits effects on the electronic band structures and the textural properties of the obtained pristine bulk *g*-C_3N_4 [55]. In this sense, Wang et al. demonstrated in 2009 that *g*-C_3N_4 was a promising visible-light photocatalyst for H_2 evolution. The as-prepared *g*-C_3N_4 achieved steady H_2 production from water containing triethanolamine as a sacrificial electron donor on light illumination ($\lambda > 420$ nm) even in the absence of noble metal co-catalysts such as Pt (4 μmol/h), opening a new

approach for the search of materials for H_2 production [56]. After this pioneering work, the scientific community has carried out a lot of work to synthesize *g*-C_3N_4 by thermal treatment of nitrogen-rich precursors such as urea, thiourea, melamine, cyanamide, and dicyandiamide, among others, to obtain *g*-C_3N_4 in different morphologies such as nanosheets or nanotubes [57,58]. However, pristine *g*-C_3N_4 presents several drawbacks for its use in photocatalysis, including a low specific surface area, insufficient visible light utilization, and, the most relevant, rapid recombination of photogenerated charge carriers [23].

3. Direct Z-Scheme Photocatalysts Based on *g*-C_3N_4

3.1. Direct Z-Scheme Photocatalysts

To compensate for the drawbacks of pristine *g*-C_3N_4 for its use in photocatalysis, as described in Section 2, a novel alternative is the design of heterojunctions, defined as the interface between two different semiconductors, which can result in suitable band alignments [59,60]. The design of type II heterojunctions using *g*-C_3N_4 is an interesting method to increase the photocatalytic efficiency by suppressing the recombination possibilities of the generated e^--h^+ pairs. In type-II heterojunction photocatalysts, the CB and the VB levels of semiconductor 1 are higher than the corresponding levels of semiconductor 2. Electron and hole pairs are separately generated in 1 and 2 subjected to light irradiation. The photogenerated electrons will transfer to semiconductor 2 while the photogenerated holes will migrate to semiconductor 1. Consequently, type II heterostructures diminish the oxidation and reduction efficiency of the isolated materials, which is the main drawback of this heterostructure (Figure 4c) [21].

Inspired by natural photosynthesis (Figure 4a), the artificial Z-scheme heterojunction design is a great alternative for the development and manufacture of novel photocatalysts, with outstanding results in numerous applications [61,62]. The Z-scheme photocatalytic system concept was proposed by Bard in 1979 for the first time [63]. Similar to what happens in photosynthesis, under light excitation, the electrons generated in a semiconductor with low reduction potential are recombined with the holes with low oxidation potential, i.e., those with the highest potential. This phenomenon generates electrons and holes isolated in the Z-scheme system with maximum redox abilities, making it the greatest advantage of these materials (Figure 4b) [34]. The traditional Z-scheme introduced by Bard [63] needs a shuttle redox mediator (electron acceptor/donor pair) to form a liquid-phase Z-scheme. Thus, Z-scheme photocatalysts suffer from the limitations of redox mediator reversibility and their specific applications, e.g., CO_2 reduction, can only be applied in the liquid phase [34]. The second generation of Z-scheme (all solid-state Z-scheme photocatalysts) was discovered in 2006 by Tada et al. [64]. These are composed of two different semiconductors with a solid-phase electron mediator as a noble metal nanoparticle (NP) or carbon material (graphene and carbon nanotubes) [65]. To solve the inconvenience of using electron mediation, Yu et al. [66] constructed a direct Z-scheme photocatalyst by combining *g*-C_3N_4 and TiO_2 in 2013. The interfacial contact between the semiconductors facilitates the direct electron transfer without the help of an electron mediator. This novel direct Z-scheme system presented the advantage of significantly reducing the construction cost [37].

In fact, *g*-C_3N_4 has received significant attention due to its potential use as a reductant semiconductor in direct Z-scheme photocatalysts given its superior chemical and physical features [26,33]. In addition, the great advantage of its use as part of Z-scheme photocatalysts is that the VB and CB positions are located at approximately +1.6 and −1.1 eV, respectively [28]. This redox potential converts *g*-C_3N_4 into an interesting reduction semiconductor for its use in several applications, such as H_2 production and CO_2 reduction (Figure 5) [67]. Nevertheless, the formation of the *g*-C_3N_4/semiconductor interface is a challenge for a Z-scheme heterostructure [33,68]. Therefore, it is necessary to design and modify novel routes of synthesis to tackle the drawbacks of these systems.

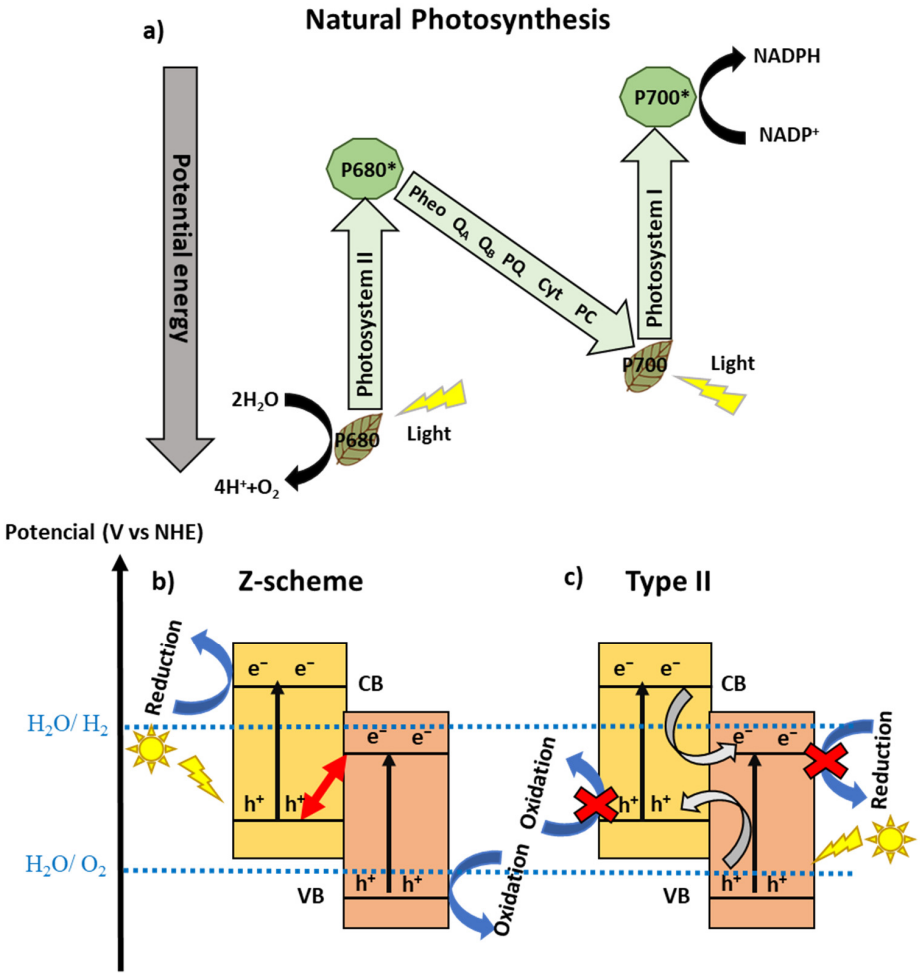

Figure 4. (**a**) Scheme of the charge separation and transformation process mechanism of natural photosynthesis. Adapted from [33]. Copyright 2019, Elsevier. (**b**) Z-scheme schematic diagram and (**c**) type II schematic diagram. Adapted from [28].

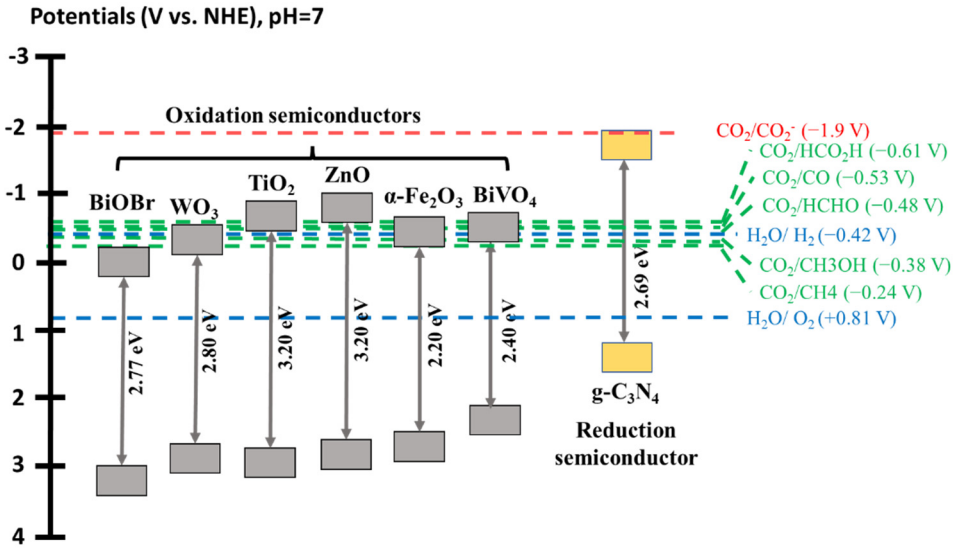

Figure 5. Band structure of *g*-C_3N_4 and some oxidation semiconductors. Adapted from [37]. Copyright 2021, Elsevier.

3.2. Synthesis and Characterization of Z-Scheme Photocatalysts Based on g-C_3N_4

Generally, the synthesis of Z-scheme photocatalysts is crucial to obtain systems with high efficiency in photocatalysis. In the literature, there are several methods to synthesize catalysts or composites such as deposition, solid-state synthesis, and hydrothermal synthesis, among others [22,37,69]. In the synthesis of Z-scheme photocatalysts, two semiconductors are combined to optimize the oxidation and reduction potential by the recombination of e^--h^+ pairs, which makes intimate contact between both semiconductors crucial [63]. To increase the activity of photocatalysts based on *g*-C_3N_4, there are several methods [58,64], such as varying the texture of *g*-C_3N_4 by means of template synthesis or deposition of metal cocatalysts. However, this section of the manuscript will focus on the synthesis of the direct Z-scheme without any mediator.

The most relevant synthetic methodologies used by the scientific community to design direct Z-scheme systems based on *g*-C_3N_4 are (Figure 6):

Solid-state synthesis. This methodology is broadly used in the synthesis of pristine *g*-C_3N_4 materials [47,70] and it is most employed to synthesize Z-scheme photocatalysts based on *g*-C_3N_4 [71]. This methodology is based on the calcination of one or a mixture of precursors in air or an inert gas atmosphere at high temperatures [72]. There are some crucial experimental parameters in the synthesis of materials using solid-state methodologies such as the heating rate, calcination temperature, and calcination time to control the crystallinity, morphology, surface properties, and phase structure of the composite [73,74]. This methodology is very interesting for the design of Z-scheme materials, as reported by W. Yu et al. [75], who synthesized *g*-C_3N_4 in the presence of pre-synthesized WO_3 to obtain a direct Z-scheme *g*-C_3N_4/WO_3 photocatalyst. Another noticeable work that uses this methodology was reported by L. Lu et al. [74]. In this work, the authors studied the effects of the calcination temperature on the photocatalytic activity of direct Z-scheme TiO_2/*g*-C_3N_4. Although this methodology is widely used in the synthesis of the *g*-C_3N_4-based direct Z-scheme, the high temperatures used and the low control of the composition are the main drawbacks.

Deposition precipitation method. This methodology is commonly used for the synthesis of photocatalysts when one of the precursors is cationic and the other is anionic. A uniform precipitated composite is formed [76,77]. The deposition precipitation technique is based on the formation of a precipitate on the surface of another component by slow addition or in situ growth of a substance, following the addition of a precipitating agent at a low temperature [78,79]. Although this methodology is not widely used in direct Z-schemes, it is an interesting methodology due to the easy fabrication of these systems [80].

Impregnation. Impregnation is another popular method for the synthesis of catalysts [81,82] and it has been used for the fabrication of Z-scheme photocatalysts [83,84]. In this approach, a solid precursor or material is in contact with a solution containing the precursor to be deposited on the solid surface. There are two methods of impregnation: (1) the wet impregnation method, in which the solid precursor is introduced with an excess volume of the second precursor solution, and (2) incipient wetness impregnation, in which the volume of the second precursor solution used is equal or less than the pore volume of the solid [82]. Due to the advantages of this methodology, Feng et al. [85] reported a composite synthesized using a simple impregnation-heating method in which MoO_3 nanoparticles were in situ supported on *g*-C_3N_4 sheets. This Z-scheme photocatalyst had photocatalytic activity in CO_2 reduction to fuels under simulated sunlight radiation. Zhou et al. [86] reported a simple impregnation method to synthesize Z-scheme *g*-C_3N_4 decorated with TiO_2 nanotubes with improved visible-light photocatalytic activity in pollutant abatement. Another example is the work of Jin et al. [84], where the authors reported the use of a one-step impregnation method to prepare direct Z-scheme $LaCoO_3$/*g*-C_3N_4 photocatalysts.

Hydrothermal synthesis. In the 21st century, hydrothermal technology is one of the preferred methods for the synthesis of materials in various interdisciplinary fields such as advanced materials technology, nanotechnology, biotechnology, etc. due to the ease of processing particles with high purity, high crystallinity, controlled stoichiometry, and con-

trolled chemical and physical characteristics, and to the environmental friendliness [87,88]. Hydrothermal processing is defined as a heterogeneous reaction performed under high temperatures and pressure in the presence of an aqueous solvent to dissolve and recrystallize substances that are relatively insoluble under ambient conditions [89]. It became one of the mostly used synthetic methodologies for the synthesis of *g*-C_3N_4-based Z-scheme photocatalysts. Jo et al. reported the synthesis of Z-scheme *g*-C_3N_4/TiO_2 photocatalysts for isoniazid degradation. Moreover, they studied the effect of the TiO_2 morphology in the synthesis of the Z-scheme photocatalysts and their catalytic activity [90]. Di et al. [91] reported the synthesis of a direct Z-scheme based on *g*-C_3N_4, synthesizing a C_3N_4/SnS_2 photocatalyst with an in situ hydrothermal method at 140 °C, and the photocatalysts had a superior visible-light CO_2 reduction performance. Recently, Lu et al. [92] reported a 2D/2D *g*-C_3N_4/$BiVO_4$ Z-scheme heterojunction using the hydrothermal methodology with remarkable photocatalytic activity enhancement of CO_2 conversion promoted by efficient interfacial charge transfer. In this sense, Wu et al. [93] synthesized 2D *g*-C_3N_4-supported nanoflower-like $NaBiO_3$ using a facile hydrothermal synthesis.

Photo-deposition methodology. Photo-deposition is a common technique for loading a cocatalyst (such as Pt NPs) onto a photocatalyst via photoreduction [94]. Photo-deposition is the phenomenon through which a cocatalyst is deposited on the surface of a semiconductor, upon illumination of a solution containing the cocatalyst precursor and the support [95]. In the last years, the scientific community has developed a great interest in the photo-deposition method to obtain Z-schemes [17,95]. One representative example is the work reported by Jiang et al. [96], where two routes for constructing the Fe_2O_3/*g*-C_3N_4 direct Z-scheme through photo-deposition were demonstrated.

The characterization of direct Z-scheme photocatalysts is crucial to identify Z-scheme heterojunctions because type II heterojunctions and Z-scheme photocatalysts have similar structures [37]. The main difference between both heterojunctions is the charge carrier mechanism, as described in Section 3.1. In the last years, researchers have studied and developed several experimental and theoretical simulation methods to characterize these novel heterostructures (Figure 6) [33,37]. The most interesting and widely used methodology to characterize and understand the mechanism of Z-scheme systems is the radical species trapping methodology [97,98]. Indeed, this methodology can be applicable because Z-scheme semiconductor 1 with a high oxidizing capacity can produce $^{\bullet}OH$ while semiconductor 2 with a sufficient reduction potential is capable of generating $O_2^{\bullet-}$ species. However, type-II heterojunction photocatalysts with a low redox (reduction or oxidation) ability can only generate one type of radicals (either $O_2^{\bullet-}$ or $^{\bullet}OH$). To elucidate this effect, the radical scavenging methodology is applied. In radical scavenging experiments, a chemical agent is introduced in the photocatalytic medium system to quench a radical, consequently decreasing the activity of the studied reaction [99,100]. Common scavengers used in the literature are tert-butyl alcohol (TBA) and isopropanol (IPA) for $^{\bullet}OH$, and N_2 gas and *p*-benzoquinone (BQ) for $O_2^{\bullet-}$ while ammonium oxalate (AO), triethanolamine (TEA), and disodium EDTA are used for holes (h^+) [100]. Other characterization techniques used to study Z-scheme systems are photoluminescence (PL) spectroscopy and electron paramagnetic resonance (EPR) spectroscopy [101–103]. During the last years, there has been an increase in the application of other spectroscopic characterization techniques such as ultraviolet photoelectron spectroscopy (UPS), transient absorption spectroscopy (TAS), surface photovoltage spectroscopy (SPS), and in situ irradiated X-ray photoelectron spectroscopy (ISI-XPS) to verify the Z-scheme charge transfer mechanism [26,104]. Another methodology used to verify Z-schemes in heterojunctions is photocatalytic reduction testing because the photogenerated electrons with adequate reduction potential in a semiconductor can be used to produce some selective products that a semiconductor with a lower reduction potential is unable to generate [33,105]. To experimentally verify the proposed system, this methodology usually needs the aid of computational calculations based on density functional theory [106–108]. In the last years, this methodology has been used to calculate the Fermi level and to interpret the charge transfer mechanism.

Finally, it is relevant to indicate that there are several methodologies used to synthesize direct Z-scheme photocatalysts, as described in this section. However, it is essential to choose and develop easy and sustainable methodologies focusing on the intimate contact between both semiconductors to obtain direct Z-scheme photocatalysts. It is also necessary to use and develop powerful characterization tools to investigate the charge-transfer mechanism to elucidate whether the heterojunctions synthesized and studied are Z-scheme photocatalyst or another heterostructure, such as type II.

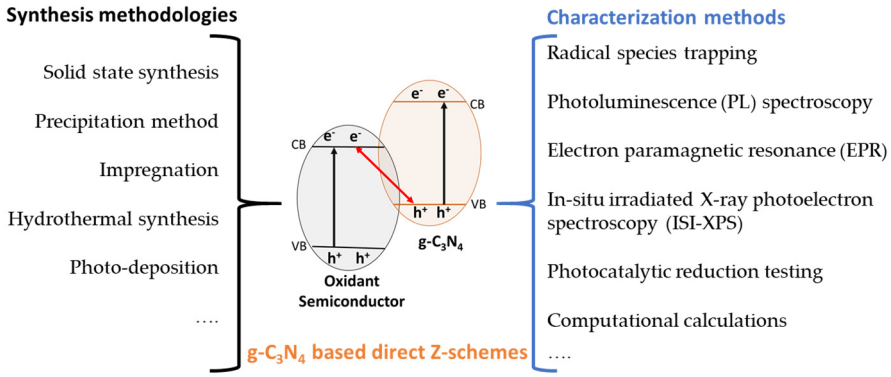

Figure 6. Scheme of representative synthesis and characterization methodologies of *g*-C_3N_4-based direct Z-schemes.

4. Environmental Applications of Direct Z-Schemes Based on *g*-C_3N_4

As mentioned in previous sections, the use of semiconductors capable of utilizing sunlight has received great interest in environmental remediation and in contributing to the solution of the energy crisis [10,109]. *g*-C_3N_4 is a semiconductor with optimal properties (absorption in visible light) for its use in this field, although it has several drawbacks [54,110], as shown in Section 2. Therefore, an alternative for *g*-C_3N_4 to be a key material in the current scenario is the use of the direct Z-scheme based on *g*-C_3N_4 [33,67]. Hence, *g*-C_3N_4-based direct Z-schemes have been widely studied by scientists for their application in photocatalytic pollutant remediation [111–113], photocatalytic H_2 production [114,115], and photocatalytic CO_2 reduction [85,116,117]. In this section, the most representative direct Z-schemes based on *g*-C_3N_4 for their use in environmental applications focusing on pollutants remediation, H_2 production, and CO_2 photoreduction will be presented. Additionally, in the main text, the most relevant aspects of the developed direct Z-schemes based on *g*-C_3N_4 for these three relevant environmental applications are described.

4.1. Pollutant Remediation

During the last decades, photocatalytic pollutant remediation has been intensively studied, leading to the synthesis of a plethora of photocatalysts active in the degradation of different pollutants. Many reports were also focused on the study of the so-called advanced oxidation processes (AOPs), which are fundamental for pollutant remediation. Indeed, AOPs include by definition the formation of highly reactive oxygen species (ROS), e.g., $O_2^{\bullet-}$, $OH^{\bullet}$, and more recently $SO_4^{2\bullet-}$ radicals, which can generate cascade processes during pollutant degradation. Indeed, these radicals have the capability of rapidly reacting with most common pollutants. This will generate radicals on the organic skeleton of the molecule and bring about defragmentation, which might lead to a complete mineralization of the contaminant in the form of CO_2 [118]. The use of heterogeneous photocatalysts can positively influence the formation of these species. As shown in Equation (1), the promotion of electrons from the VB to the CB origins holes, which might react with water or $SO_2O_8^{2-}$ for the generation of $OH^{\bullet}$ (see Equations (2) and (3)) or $SO_4^{2\bullet-}$ radicals (Equation (4)), respectively, which participate in the subsequent radical reaction pathway for pollutant degradation [119,120]. On the other hand, the electrons accumulated at the CB might react

with O_2 to generate $O_2^{\bullet -}$ radicals (Equation (5)), fundamental for the following cascade reactions [121]:

$$SC + h\nu \rightarrow e_{CB}^{-} + h_{VB}^{+} \quad (1)$$

$$h_{VB}^{+} + OH_{surface}^{-} \rightarrow OH^{\bullet} \quad (2)$$

E^0 = 2.8 V (V vs. NHE, pH 7, 25 °C, 1 atm)

$$h_{VB}^{+} + H_2O_{absorbed} \rightarrow OH^{\bullet} + H^{+} \quad (3)$$

$$h_{VB}^{+} + S_2O_{8\ adsorbed}^{2-} \rightarrow SO_4^{\bullet -} \quad (4)$$

E^0 = 2.6 V (V vs. NHE, pH 7, 25 °C, 1 atm)

$$e_{CB}^{-} + O_{2\ absorbed} \rightarrow O_2^{\bullet -} \quad (5)$$

E^0 = −0.33 V (V vs. NHE, pH 7, 25 °C, 1 atm)

As mentioned in the text, the use of heterojunctions plays a key role in overcoming the main drawbacks of photocatalysts. Thus, the oxidation processes involved in the formation of ROS might be more favored by the composite than its isolated components [122]. The coupling of *g*-C_3N_4 with different semi-conductors gives birth to an extended family of direct Z-scheme heterojunctions, active in AOPs (Figure 7) and, subsequently, applied in pollutant remediation [67].

In the following pages, we will analyze some of the most important examples of pollutant photodegradation by direct Z-schemes based on *g*-C_3N_4. Mainly, we will focus on some of the most representative pollutants used in photodegradation studies and some of the most illustrative results are summarized in Table 1.

Among the different pollutants, rhodamine B (RhB) is one of the most widely studied in recent reports related to this topic. Indeed, this water-soluble molecule is used as a red dye in the textile industry, thus representing one of the most concentrated wastes in water. Being classified as carcinogenic, RhB must be removed from the residual water, and this can be achieved by the use of photocatalysis [123]. Metal-free *g*-C_3N_4-based direct Z-scheme photocatalysts have been extensively applied in the degradation of RhB with highly remarkable results. M. Tang et al. [124] developed a ternary system composed of AgI/Ag_3PO_4/*g*-C_3N_4 with high activity in the degradation of RhB and a neonicotinoid pesticide due to the low recombination rate assured by the presence of the three compounds, as shown in Figure 8a. Indeed, the use of isolated components or even binary systems containing these materials did not lead to the same high yield in degradation. This finding was also demonstrated by Y. He et al. [116] using SnO_{2-x}/*g*-C_3N_4 composite in RhB degradation. Figure 8b depicts another advantage of this heterostructure, i.e., an increase in the surface area, which is known to be one of the main drawbacks of the application of *g*-C_3N_4 in catalysis [116]. Another noteworthy example is the 2D/2D SnS_2/*g*-C_3N_4 heterostructure developed by H. Che et al. [125], where the efficiency of the charge carrier separation is enhanced by the high interfacial contact area generated from the contact between the 2D materials. In addition, the photocatalytic activity of this catalyst is boosted because both $OH^{\bullet}$ and $O_2^{\bullet -}$ radicals might be generated, as presented in Figure 8c [126]. Considering lower dimensionality systems, 0D materials have found applicability in the generation of novel composites. For example, Y. Fu et al. [111] developed the MoS_2 QD/*g*-C_3N_4 heterostructure and demonstrated that the interaction between the 0D QD and 2D moieties can stabilize the QDs. Photocurrent measurements (Figure 8d) highlight that in the composites, the interfacial charge transfer is faster and the recombination of photoexcited charges is inhibited, thus boosting the photocatalytic activity in RhB degradation.

Tetracycline (TC) is a common antibiotic but with many side effects to live bodies. Its wide usage in husbandry (cattle, swine, poultry, and fishery) leads to an increase in its concentration in water and poses a threat to the natural balance. Among other degradation techniques, photocatalysis has found application in the degradation of this molecule [127–129],

and g-C_3N_4-based direct Z-scheme photocatalysts have been extensively applied for this purpose. One recent report developed by J. Kang et al. [130] shows how the construction of the heterostructure g-C_3N_4/Na-$BiVO_4$ can boost the photodegradation of TC, promoted in this case by the formation of peroxymonosulfate radical. Indeed, the calculated CB and VB presented in Figure 9a demonstrate that the use of g-C_3N_4 can overcome one of the main drawbacks of the promising photocatalyst $BiVO_4$, i.e., the low CB potential. Similarly, peroxymonosulfate-mediated TC photodegradation was demonstrated by C. Jin et al. [131] to be successful when using the 2D/2D Co_3O_4/g-C_3N_4 heterostructure. In this case, the two-dimensionality allows a better separation and transfer of the charges, as demonstrated by the photoluminescence measurements in Figure 9b. In addition, S. Wang [132] et al. showed that the use of α-Fe_2O_3/g-C_3N_4 in TC degradation could improve the photocatalytic activity of the isolated components due to the formation of interfacial -NH/-NH_2 groups on the g-C_3N_4 surface. The synergy between the two components is determined by the fact that the defect-rich g-C_3N_4 improves the absorption of visible light on the material and α-Fe_2O_3 diminishes the recombination rate.

RhB and TC represent two of the most common pollutants that have been studied in photodegradation processes, but, certainly, according to the latest publications, there are other dangerous pollutants, which are present worldwide in high concentrations in water [133]. Consequently, photocatalysts based on g-C_3N_4 have also been used for the degradation of different pharmaceutical products or persistent organic pollutants (POPs), e.g., fluoroquinolone antibiotics, benzodiazepines, or parabens. Y. Zhou et al. [134] successfully used a 3D/2D MOF-derived $CoCeO_x$/g-C_3N_4 Z-scheme heterojunction in the photocatalytic degradation of carbamazepine. The presence of the MOF-derived $CoCeO_x$ increased the surface area, overcoming one of the main drawbacks of g-C_3N_4. Additionally, J. Huang et al. [135] showed that the combination of g-C_3N_4 and TiO_2 originated an active photocatalyst for the visible-light elimination of enrofloxacin in water, as indicated in Figure 9c. In this case, the presence of g-C_3N_4 favors the absorbance of TiO_2 under visible light, giving more applicability to the well-known photocatalyst TiO_2. Furthermore, J. Meng et al. [136] synthesized the WO_3/g-C_3N_4 heterojunction for the degradation of methylparaben. In this case, the heterostructure avoids the fast recombination typical in both materials and the presence of g-C_3N_4 enhances the formation of $O_2^{\bullet-}$ radicals, which are involved in the degradation process (Figure 9d).

In summary, direct Z-schemes are a great alternative to improve the catalytic activity of bare photocatalysts in pollutant abatement, obtaining total conversion in a few hours. However, it is necessary to test the photocatalysts under more realistic conditions since most of the catalytic tests were performed with isolated pollutants in pure water.

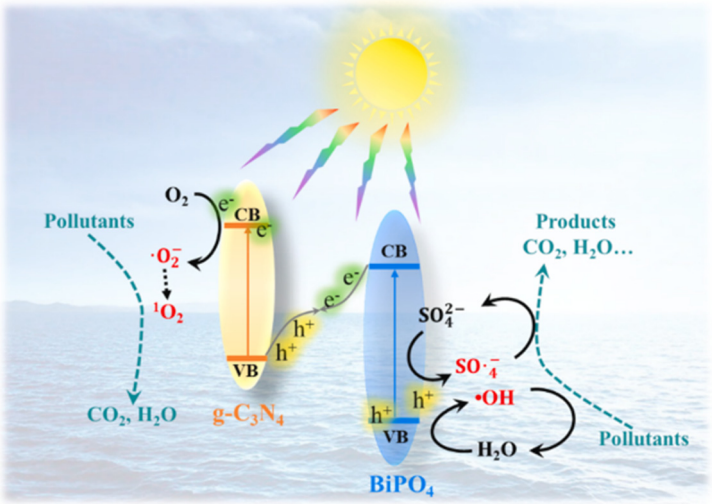

Figure 7. ROS formation catalyzed by a heterostructure. Reproduced from [137]. Copyright 2022, Elsevier.

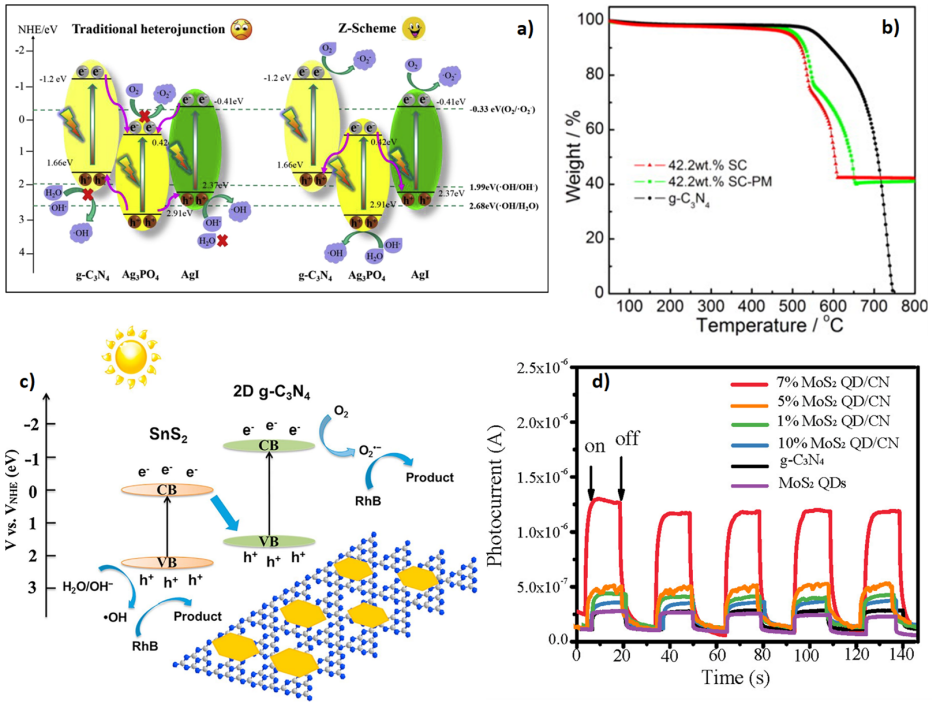

Figure 8. (**a**) Photocatalytic mechanism in the presence of the $AgI/Ag_3PO_4/g\text{-}C_3N_4$ heterostructure. Reproduced from [124]. Copyright 2020, Elsevier. (**b**) TG profiles of $g\text{-}C_3N_4$, its composite with $SnO_{2\text{-}x}$ (SC), and their physical mixture (SC-PM). Reproduced from [116]. Copyright 2015, Elsevier. (**c**) Proposed photocatalytic mechanism for the degradation of RhB by $SnS_2/g\text{-}C_3N_4$. Reproduced from [126]. Copyright 2019, Elsevier. (**d**) Transient photocurrent response of $g\text{-}C_3N_4$ and MoS_2 QD/$g\text{-}C_3N_4$ composites. Reproduced from [111]. Copyright 2017, Elsevier.

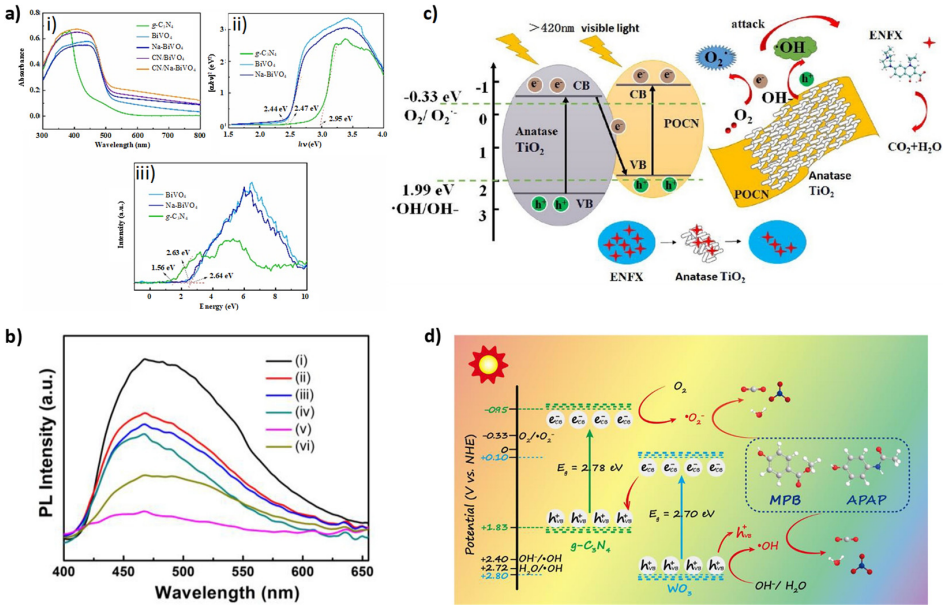

Figure 9. (**a**) UV–vis DRS spectra (i) and Mott–Schottky plots (ii) of catalysts, XPS valence spectra (iii) of $g\text{-}C_3N_4$, $BiVO_4$, and Na-$BiVO_4$. Reproduced from [130]. Copyright 2021, Elsevier. (**b**) Photoluminescence spectra: (i) $g\text{-}C_3N_4$, (ii) 1%$Co_3O_4/g\text{-}C_3N_4$, (iii) 3%$Co_3O_4/g\text{-}C_3N_4$, (iv) 5%$Co_3O_4/g\text{-}C_3N_4$, (v) 10%$Co_3O_4/g\text{-}C_3N_4$, and (vi) 15%$Co_3O_4/g\text{-}C_3N_4$. Reproduced from [131]. Copyright 2020, Elsevier. (**c**) Proposed visible-light photocatalytic enrofloxacin degradation mechanism by $g\text{-}C_3N_4/TiO_2$. Reproduced from [135]. Copyright 2020, Elsevier. (**d**) Charge carrier transfer mechanism in the presence of $WO_3/g\text{-}C_3N_4$ direct Z-scheme photocatalyst. Reproduced from [136]. Copyright 2021, Elsevier.

Table 1. g-C_3N_4-based direct Z-scheme photocatalysts for pollutant remediation.

Z-Scheme Photocatalyst	Fabrication	Irradiation Source	Pollutant/Photodegradation Performance/Reaction Time (min)	Reference
SnO_{2-x}/*g*-C_3N_4	solid state	350W Xenon lamp (420 nm < λ < 800 nm)	RhB/100%/60 min	[116]
MoS_2 QD/*g*-C_3N_4	microemulsion method	350W Xenon lamp (λ > 420 nm)	RhB/100%/9 min	[111]
Bi_3O_4Cl/*g*-C_3N_4	solid phase calcination method	250W Xenon lamp (λ > 420 nm)	RhB/98.3%/90 min	[125]
β-Bi_2O_3/*g*-C_3N_4	sonication	350W Xenon lamp (λ > 420 nm)	RhB/98%/80 min	[138]
g-C_3N_4/ZnO	thermal atomic layer deposition	300W Xenon lamp	Cephalexin/92.7%/60 min	[139]
SnS_2/*g*-C_3N_4	solvothermal method	300W Xenon lamp (λ > 400 nm)	RhB/94.8%/60 min	[126]
Fe_3O_4-OQs/Bi_2O_4/*g*-C_3N_4	hydrothermal method	250W Xenon lamp (λ > 420 nm)	RhB/92.7%/160 min	[140]
g-C_3N_4/TiO_2	solvent evaporation method	500 W Xenon lamp	RhB/100%/20 min	[141]
α-Fe_2O_3/*g*-C_3N_4	calcination	100W LED lamp (λ = 420 nm)	Tetracycline/95.0%/60 min	[142]
ZnO/*g*-C_3N_4	hydrothermal method	Visible light	Atrazine/90%/180 min	[143]
Co_3O_4/*g*-C_3N_4	solid state	300W Xenon lamp (λ > 420 nm)	Tetracycline/90.0%/60 min	[131]
AgI/Ag_3PO_4/*g*-C_3N_4	in situ ion exchange method	300W Xenon lamp (λ > 420 nm)	Nitenpyram/100%/4 min	[124]
g-C_3N_4/anatase TiO_2	calcination	350W Xenon lamp (λ > 420 nm)	Enrofloxacin/98.5%/60 min	[135]
g-C_3N_4/Na-$BiVO_4$	hydrothermal method	300W Xenon lamp (λ > 420 nm)	Tetracycline/98.2%/40 min	[130]
WO_3/*g*-C_3N_4	hydrothermal method	300W Xenon lamp (λ > 400 nm)	MPB/98.2%/60 min	[136]
ZnO/*g*-C_3N_4	hydrothermal method	Solar light	Rh B/98%/100 min	[144]
α-Fe_2O_3/*g*-C_3N_4	sonication	500 W Xenon lamp	Tetracycline/97.1%/80 min	[132]
$CoCeO_x$/*g*-C_3N_4	solid state	300W Xenon lamp (λ > 420 nm)	Carbamazepine/90.1%/60 min	[134]

4.2. H_2 Production

One of the greatest current challenges of our society from an environmental and energy point of view is the production and use of clean fuel from renewable energies [2,145]. During the last decades, H_2 has become a highly relevant alternative to fossil fuels because it has clean combustion and high energy density [145]. Therefore, it is essential to develop technologies to allow the production of H_2 without using fossil fuels [146]. This subsection is placed here, as the water splitting uses similar starting radicals to pollutant abatement in aqueous ambience. The generation of H_2 by water splitting using sunlight has received great interest from the scientific community and in society [147,148]. The water splitting reaction that generates H_2 and O_2 (Equation (6)) is a non-spontaneous endergonic reaction (ΔG = +237 KJmol^{-1}), which means that energy is needed for the reaction to occur [148]:

$$H_2O \rightarrow {}^1/_2O_2 + H_2 \left(\Delta G = 237 \text{ KJmol}^{-1}\right) \quad (6)$$

One alternative to the generation of H_2 from water splitting is the use of photocatalysis, which would require the use of sunlight and a semiconductor (photocatalysis). For the reaction to occur, the CB potential of the semiconductor should be more negative than

the reduction potential of H_2O (0 V vs. NHE) for H_2 generation, and the VB potential of the semiconductor should be more positive than the oxidation potential of H_2O (1.23 V vs. NHE) for O_2 generation [148,149]. An interesting semiconductor for this reaction is *g*-C_3N_4 since the VB and CB positions are located at approximately +1.6 and −1.1 eV, respectively, with a band gap of ~2.7 eV, making the reaction of water splitting possible using sunlight [56,150]. However, the *g*-C_3N_4 photocatalyst presents low activity in water splitting [23], as mentioned in Section 2. To solve this low activity of *g*-C_3N_4 in water splitting, the scientific community has focused on studying heterojunctions based on *g*-C_3N_4 [26,60]. A heterojunction that has aroused the interest of the scientific community is the direct Z-scheme because the latter is present in the systems responsible for the water splitting reaction in photosynthesis due to the decrease in the e^--h^+ pair recombination rate [38,98]. This makes the direct Z-schemes promising systems, which may lead to adequate quantum efficiency values for their commercialization [38]. In this subsection, several direct Z-scheme photocatalysts based on *g*-C_3N_4 in different conditions used in water splitting are summarized in Table 2. In addition, a detailed discussion of the most relevant Z-scheme photocatalysts from the point of view of the catalytic activity and reaction mechanism will be described in the main text.

R. Ye et al. [151] described a $CoTiO_3$/*g*-C_3N_4 novel Z-scheme heterostructure photocatalyst for H_2 evolution (858 μmol g^{-1} h^{-1}) under visible light with effectively intimate interfaces linked through the Co–O–N or Ti–O–N bonds, as shown in Figure 10a. The authors showed that this system presents a direct Z-scheme mechanism by PL, PEC, and ESR analyses. The work described by R. Ye et al. focusing on Z-scheme $CoTiO_3$/*g*-C_3N_4 was useful for further development of novel heterojunction photocatalytic systems based on perovskite, polymer, and composite photocatalysts for photocatalytic H_2 production. X. She et al. [152] showed a novel strategy for the synthesis of an α-Fe_2O_3/2D *g*-C_3N_4 Z-scheme hybrid structure containing ultrathin *g*-C_3N_4 platelets. In the synthesis methodology used in this study, α-Fe_2O_3 promotes the formation of *g*-C_3N_4 nanosheets. Moreover, the authors claimed that the Fe_2O_3/2D *g*-C_3N_4 direct Z-scheme photocatalyst exhibits unprecedented photocatalytic activity toward H_2 evolution (31,400 μmol g^{-1} h^{-1}), with a remarkably high quantum efficiency of 44.35% at a wavelength of 420 nm, as shown in Figure 10b. The enhanced performance of H_2 evolution in α-Fe_2O_3/2D *g*-C_3N_4 was attributed to the 2D structure of *g*-C_3N_4, allowing an efficient transfer of the photoexcited electron to the reactant. Another factor relevant to improving the photocatalytic activity of this system is the Z-scheme structure due to the low electron-hole recombination in both α-Fe_2O_3 and 2D *g*-C_3N_4 and the close interface contact between α-Fe_2O_3 and 2D *g*-C_3N_4, enabling fast electron transfer from the conduction band of α-Fe_2O_3 to the valence band of 2D *g*-C_3N_4. This work shows that the dimensionality (2D) and the porous hierarchy of the systems present a great effect on the photocatalytic activity of Z-schemes. Moreover, Fe_2O_3/2D *g*-C_3N_4 direct Z-scheme photocatalysts exhibit great values in H_2 production, indicating the effectivity and interest of these artificial Z-schemes for their use in this application. Considering the effect of the 2D materials, Y. Yang, et al. [153] designed and constructed a direct Z-scheme van der Waals heterojunction composed of ultrathin $WO_3 \cdot H_2O$ and *g*-C_3N_4 nanosheets using simple hydrothermal synthesis to achieve efficient water splitting without the addition of any sacrificial agents (482 μmol g^{-1} h^{-1}). This $WO_3 \cdot H_2O$/*g*-C_3N_4 system could efficiently transport the electrons, decreasing the e^--h^+ recombination rates, as shown in Figure 10c, which led to a considerable improvement in the photocatalytic performance. Another relevant parameter in the study of Z-schemes is the presence of interfacial defects since they might be beneficial to the recombination of interfacial photogenerated e^-/h^+ and could serve as Z-scheme pathways for charge transfer. L. Kong et al. [154] fabricated a direct Z-scheme *g*-C_3N_4/Ti^{3+}-doped TiO_2 to show this effect. The authors observed that the Ti^{3+} defects were introduced under CB of TiO_2, which improved the interfacial charge transfer channels for Z-scheme *g*-C_3N_4/Ti^{3+}-doped TiO_2 composite and improved the visible light absorption. These properties were studied using a radical species trapping methodology, UV-Vis spectroscopy, and EPR analysis. Due to the

enhanced properties, this system has high activity (1938 μmol·h^{-1}·g^{-1}) under simulated solar light and good stability in photocatalytic H_2 evolution. S. Qin et al. [155] showed a promising way to construct Z-scheme heterostructures based on metal-organic cages (MOCs) and semiconductors for their use in photocatalytic H_2 generation. The authors synthesized an MOC, integrating four organic photosensitized ligands M^{4-} and two Pd^{2+} catalytic centers. Then, the MOC was successfully immobilized by hydrogen bonds to obtain a robust heterogeneous direct Z-scheme *g*-C_3N_4/MOC-Q1 (Figure 10e). This innovative system presents high H_2 evolution activity (4495 μmol g^{-1} h^{-1}). In this manuscript, it was described that Z-scheme systems improved the photocatalytic H_2 production rate, but, on the other hand, the photoconversion efficiency is still far from the requirement for practical applications.

One novel methodology based on direct Z-scheme system photocatalysts is the design of dual-Z-scheme systems that ensure the efficient transmission of photogenerated carriers and further optimize the structure of the Z-scheme system. Y. Yang et al. [114] successfully constructed an efficient dual-Z-scheme heterojunction, CdS/$W_{18}O_{49}$/*g*-C_3N_4 (CWOCN), by introducing CdS nanoparticles in the $W_{18}O_{49}$/*g*-C_3N_4 (WOCN) composite. This dual-Z-scheme system exhibits extraordinary photocatalytic activity and stability. The TRPL measurement results demonstrated that the formation of a dual-Z-scheme system facilitates the transmission of photogenerated electrons and prolonged the electrons' lifetime, thus boosting the photocatalytic activity. It led to a prominent photocatalytic H_2 evolution rate (11,658 μmol h^{-1} g^{-1}). This study offers guidance for exploiting and designing efficient and practical photocatalysts.

To conclude this section, there are several methodologies based on direct Z-scheme system photocatalysts used to obtain photocatalysts that are active in H_2 production. However, this technology is far from commercialization due to the low reproducibility of the materials and low quantum efficiency.

Table 2. Summary of direct Z-scheme photocatalysts based on *g*-C_3N_4 for water splitting.

Z-Scheme Photocatalyst	Fabrication Methodology	Irradiation Source	H_2 Production Activity (μmol g^{-1} h^{-1}) and AQE	Reference
$CoTiO_3$/*g*-C_3N_4	Solid-State	Xenon lamp (300 W, λ ≥ 420 nm)	858 AQE: 38.4% (365 nm)	[151]
g-C_3N_4/ZnO	Deposition	Xenon lamp (300 W, λ ≥ 420 nm)	322	[156]
g-C_3N_4/PSi	Polycondensation reaction	Xenon lamp (300 W, λ ≥ 400 nm)	870	[157]
2D α-Fe_2O_3/*g*-C_3N_4	Solid-State	Xenon lamp (300 W, λ ≥ 420 nm)	31400 AQE: 44.35% (420 nm)	[152]
WO_3.H_2O/*g*-C_3N_4	Hydrothermal method	Xenon lamp (300 W, λ > 400 nm)	482 AQE: 6.2% (420 nm)	[153]
g-C_3N_4/Ti^{3+}-TiO_2	Solid-State	Xenon lamp (300 W, λ > 400 nm)	1938	[154]
Nb_2O_5/*g*-C_3N_4	Hydrothermal	Xenon lamp (1000 W, 1.5G)	110,000	[115]
$Bi_2O_2CO_3$/*g*-C_3N_4	Heat treatment method	Xenon lamp (300 W, λ ≥ 400 nm)	965 AQE: 7.14% (420 nm)	[158]
2D/2D *g*-C_3N_4/Sn_3O_4	Calcined in N_2	Xenon lamp (300 W, λ ≥ 400 nm)	1960	[159]
g-C_3N_4/MOC-Q1	Deposition	Xenon lamp (300 W, λ ≥ 420 nm)	4495 AQE: 0.50% (425 nm)	[155]
CdS/$W_{18}O_{49}$/*g*-C_3N_4 (CWOCN)	Chemical bath deposition	Xenon lamp (300 W, λ ≥ 420 nm)	11,658 AQE: 26.73% (420 nm)	[116]
Cu_2O/*g*-C_3N_4	Solid-State	Xenon lamp (300 W, λ ≥ 420 nm)	266.3 AQE: 13.40% (420 nm)	[160]

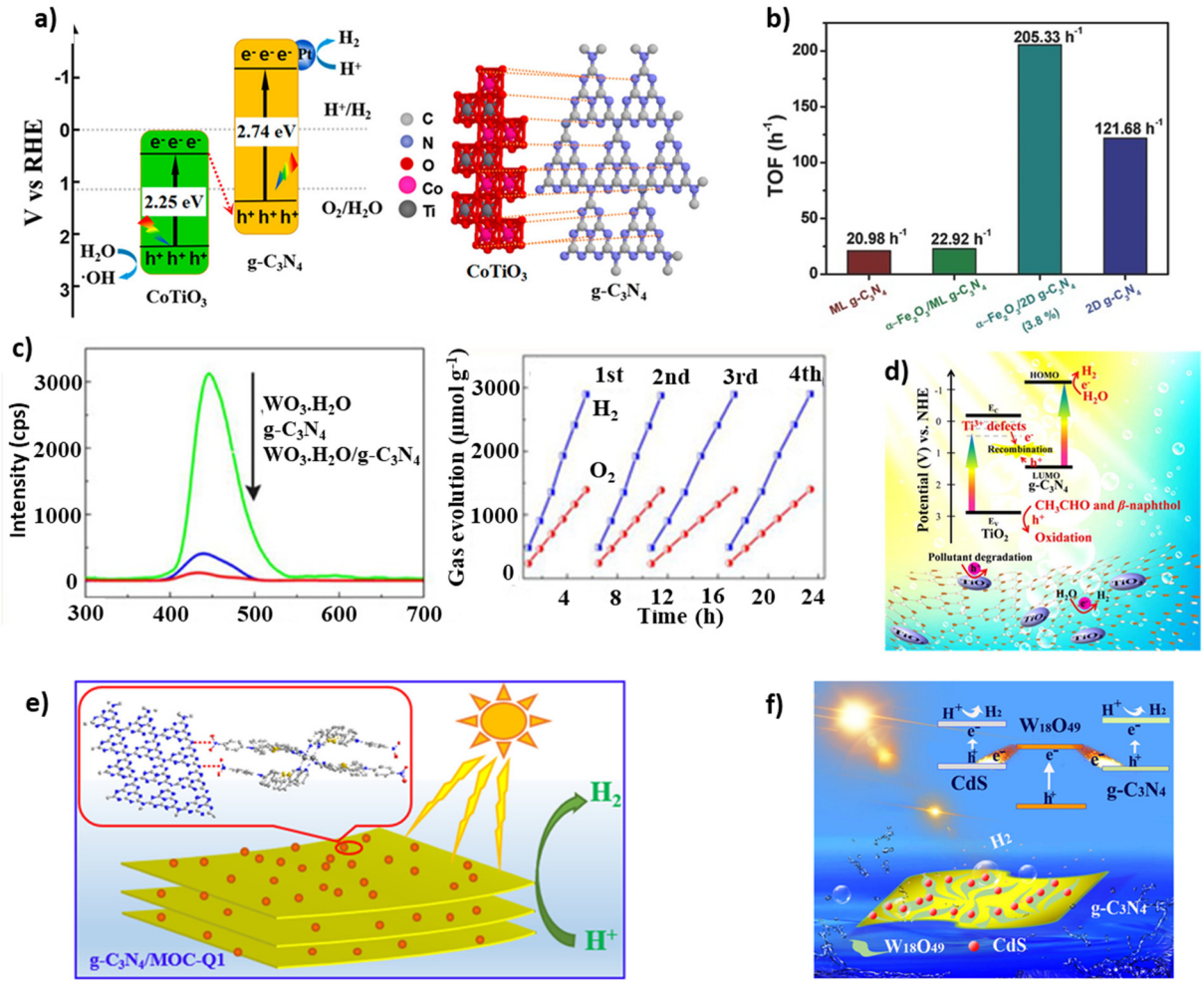

Figure 10. (**a**) Schematic illustration of the mechanisms for charge carrier separation of $CoTiO_3$/*g*-C_3N_4 direct Z-schemes and the molecular interaction between $CoTiO_3$ and *g*-C_3N_4 through the formation of chemical bonds. Reproduced from [151]. Copyright 2016, ACS Publications. (**b**) Catalytic activity (Turnover frequency) of ML *g*-C_3N_4, α-Fe_2O_3/ML *g*-C_3N_4, 2D *g*-C_3N_4, and α-Fe_2O_3/2D *g*-C_3N_4 for water splitting. Reproduced from [152]. Copyright 2017, Willey. (**c**) PL spectra of *g*-C_3N_4, $WO_3 \cdot H_2O$, and $WO_3 \cdot H_2O$/*g*-C_3N_4 and visible-light-driven photocatalytic H_2 and O_2 generation for $WO_3 \cdot H_2O$/*g*-C_3N_4. Reproduced from [153]. Copyright 2018, Willey. (**d**) Schematic diagram of the mechanism for the separation and transfer of photoinduced charge carrier in CN-T-H composite. Reproduced from [154]. Copyright 2018, Elsevier. (**e**) Schematic illustration of a heterostructure of *g*-C_3N_4/MOC-Q1. Reproduced from [155]. Copyright 2021, ACS Publications. (**f**) The mechanism of dual-Z-scheme heterojunction (CWOCN) for H_2 production. Reproduced from [114]. Copyright 2021, Willey.

4.3. CO_2 Photoreduction

The great use of fossil fuels in the last decades has led to significant CO_2 emissions into the atmosphere, resulting in global warming responsible for climate change, which represents one of the greatest challenges of the current society [161,162]. An innovative alternative to reduce the emissions of CO_2 into the atmosphere would be to capture CO_2 [163] and transform it into high value-added products using sunlight, mimicking natural photosynthesis [164]. However, CO_2 is a stable covalent molecule due to the C=O bond, resulting in high dissociation energy (531 kJ mol^{-1}) [165]. CO_2 photoreduction is an alternative method to break the C=O bond using solar energy. Nevertheless, this process is a multielectron transfer process, which may result in a great variety of products with

different carbon oxidation states, including CH_4, CH_3OH, HCHO, HCOOH, and CO [166] (see Equations (7)–(13)):

$$CO_2 + 2e^- \rightarrow CO_2^{\cdot -} \quad (7)$$

$E^0 = -1.90$ V (V vs. NHE, pH 7, 25 °C, 1 atm)

$$CO_2 + 2H^+ + 2e^- \rightarrow HCOOH \quad (8)$$

$E^0 = -0.61$ V (V vs. NHE, pH 7, 25 °C, 1 atm)

$$CO_2 + 2H^+ + 2e^- \rightarrow CO + H_2O \quad (9)$$

$E^0 = -0.53$ V (V vs. NHE, pH 7, 25 °C, 1 atm)

$$CO_2 + 4H^+ + 4e^- \rightarrow HCHO + H_2O \quad (10)$$

$E^0 = -0.48$ V (V vs. NHE, pH 7, 25 °C, 1 atm)

$$CO_2 + 6H^+ + 6e^- \rightarrow CH_3OH + H_2O \quad (11)$$

$E^0 = -0.38$ V (V vs. NHE, pH 7, 25 °C, 1 atm)

$$CO_2 + 8H^+ + 8e^- \rightarrow CH_4 + 2H_2O \quad (12)$$

$E^0 = -0.24$ V (V vs. NHE, pH 7, 25 °C, 1 atm)

$$2H_2O + 2e^- \rightarrow 2OH^- + H_2 \quad (13)$$

$E^0 = -0.41$ V (V vs. NHE, pH 7, 25 °C, 1 atm)

Another challenge in the photocatalytic reduction of CO_2 is that the reduction of H_2O to H_2 (see Equation (1)) has a similar reduction potential to the reduction of CO_2. This fact means that in the aqueous ambience, there is competition between both reactions [167]. To overcome the challenges presented above in the reduction of CO_2, the scientific community has focused on designing selective photocatalysts for the reduction of CO_2 to various high value-added products [168]. Among the different photocatalysts developed, *g*-C_3N_4 should be highlighted. G. Dong et al. reported that pristine *g*-C_3N_4 without any cocatalyst presented selectivity in the photocatalytic reduction of CO_2 into CO under visible-light irradiation in the presence of water vapor [169]. However, the efficiency of this photocatalyst was low due to the high e^--h^+ pair recombination rate [47]. As mentioned throughout this review, an alternative used to reduce the e^--h^+ recombination ratio, which is one of the challenges of *g*-C_3N_4, is the design and synthesis of heterojunctions [26]. Within the use of heterojunctions for the photoreduction of CO_2, artificial direct Z-scheme photocatalysts have received great interest from the scientific community since these systems mimic the electronic processes that occur in photosynthesis to reduce CO_2 into hydrocarbons [33,34]. Therefore, the study of these artificial systems for the reduction of CO_2 has grown noticeably in the last years, being a key approach to understanding the photocatalytic mechanism and to design efficient systems capable of being marketed [39,170,171]. In this subsection, several direct Z-scheme photocatalysts based on *g*-C_3N_4 used in CO_2 photoreduction are summarized in Table 3. In addition, a detailed discussion of the most relevant photocatalyst Z-scheme from a synthesis, catalytic activity, and reaction mechanism perspective will be described in the main text.

W. Yu et al. [172] described the coupling effect of ZnO for the improved photoactivity of *g*-C_3N_4 and the authors also proposed a direct Z-scheme mechanism to explain the better performances of the *g*-C_3N_4/ZnO binary composite photocatalytic system. The *g*-C_3N_4/ZnO photocatalytic system exhibited enhanced photocatalytic activity for CO_2 reduction compared with pure *g*-C_3N_4, with selectivity towards CH_3OH. This enhancement of photocatalytic CO_2 reduction activity is attributed to the highly efficient ZnO-to-*g*-C_3N_4

electron transfer occurring at the intimate contact interface between the *g*-C_3N_4 and ZnO phases. This work provided new insights into the rational construction of a *g*-C_3N_4-based photocatalytic system and the design of a direct Z-scheme system without an electron mediator for the photocatalytic CO_2 reduction reaction. To enhance the photocatalytic activity of the materials, Z. Jiang et al. [170] described that the Z-scheme hybrid material should present several characteristics to accelerate the reduction process, including a 3D hierarchical structure and preferably basic sites, which promote CO_2 adsorption. In addition, these systems should present an efficient separation of the e^--h^+ pairs and an enhancement in the reduction character of electrons in the conduction band of *g*-C_3N_4. In this work, a hierarchical direct Z-scheme hybrid was developed by combining 3D urchin-like α-Fe_2O_3 and *g*-C_3N_4 photocatalysts (Figure 11a) for the photocatalytic reduction of CO_2 without the use of any sacrificial agent or cocatalyst. The hierarchical system improved the photocatalytic reduction of CO_2 to form CO (27.2 μmol g^{-1} h^{-1}), and the system was stable for four cycles (Figure 11a). N.T. Thanh Truc et al. [173] synthesized a Nb-TiO_2/*g*-C_3N_4 direct Z-scheme system, in which the photo-excited e^- in the CB of the Nb-TiO_2 combines with the photo-excited h^+ in the VB of the *g*-C_3N_4, preserving the existence of e^- in the CB of the *g*-C_3N_4 and h^+ in the VB of Nb-TiO_2. Thus, the established Nb-TiO_2/*g*-C_3N_4 direct Z-scheme system produced a huge amount of available e^-/h^+ pairs for the reduction of CO_2 into various valuable fuels. Moreover, the authors observed that the photo-current response of the prepared Nb-TiO_2/*g*-C_3N_4 (~57.55 μA/cm^2) was much higher than that of *g*-C_3N_4 (~3.92 μA/cm^2) and Nb-TiO_2 (~12.41 μA/cm^2) under the full visible light spectrum (Figure 11b). This result showed that the photo-excited e^- in the CB of the Nb-TiO_2 tends to combine with photo-excited h^+ in the VB of the *g*-C_3N_4, preserving the existence of e^- in the CB of the *g*-C_3N_4 and h^+ in the VB of the Nb-TiO_2, indicating the power of this characterization technique to address the Z-scheme mechanism. M. Lu et al. [92] synthesized 2D/2D ultrathin nanosheets of *g*-C_3N_4/$BiVO_4$ Z-scheme heterojunction via thermal-polymerization and a subsequent hydrothermal method. The 2D/2D *g*-C_3N_4/$BiVO_4$ ultrathin nanosheets exhibited a great photocatalytic evolution rate for CO (145 μmol g^{-1} h^{-1}) and CH_4 (133 μmol g^{-1} h^{-1}) (Figure 11c). The study presented by Lu et. al. evidenced the relevance of using 2D materials. Indeed, the direct Z-scheme heterojunction and face-to-face interfacial contact between 2D *g*-C_3N_4 and 2D $BiVO_4$ accelerated the charge transfer and separation, improving the catalytic activity of these systems in CO_2 reduction. B. Tahir et al. [117] designed 3D/2D WO_3/*g*-C_3N_4 microspheres with an effective interfacial contact using a facile single-step hydrothermal method. The direct growth of WO_3 microspheres with *g*-C_3N_4 enables good interaction among both semiconductors, enabling proficient charge carrier separation (Figure 11d). The synergistic effect with the larger interfacial contact area and proficient charge carrier separation of this system improves the CO and CH_4 production over WO_3/*g*-C_3N_4 (145 and 133 μmol g^{-1} h^{-1}, respectively), which are 2- and 4-fold higher than the use of pristine *g*-C_3N_4. This work reveals that effective interfacial contact between both semiconductors present on the Z-scheme photocatalyst is a key factor to promoting the photocatalytic CO_2 conversion to solar fuels under visible light irradiation. J. Zhao et al. [174] showed the development of a novel direct Z-scheme $Bi_{19}S_{27}Br_3$/*g*-C_3N_4 composite using the ionic liquid-assisted solvent-thermal method. The $Bi_{19}S_{27}Br_3$/*g*-C_3N_4 composites showed enhanced CO_2 photoreduction activity for the production of CO (12.87 μmol g^{-1} h^{-1}). The authors observed in this work that the C-S bond boosts the transfer of photogenerated charge between $Bi_{19}S_{27}Br_3$ and *g*-C_3N_4, as shown in Figure 11e. Therefore, the construction of a chemical bond-bridged direct Z-scheme is a promising strategy for precisely tailoring the photogenerated charge separation direction of the photocatalyst.

In conclusion, although the synthesis of Z-schemes has been successfully achieved and they are active in CO_2 photoreduction, nowadays, the photocatalytic efficiencies of Z-schemes are still too low for their commercialization.

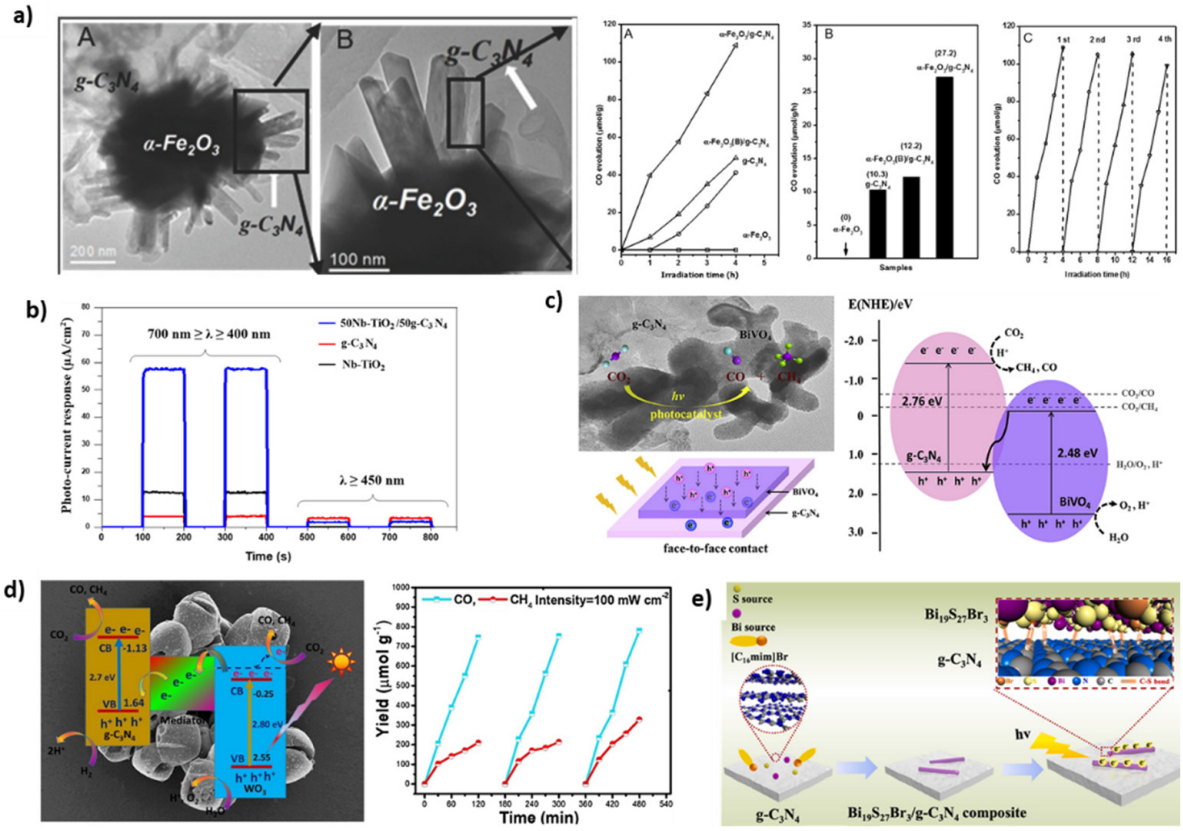

Figure 11. (**a**) TEM images of α-Fe_2O_3/*g*-C_3N_4 (A) and high magnitude TEM images of α-Fe_2O_3/*g*-C_3N_4 (B). Time courses of photocatalytic CO evolutions (A), average CO production rates of *g*-C_3N_4, α-Fe_2O_3 (B), and α-Fe_2O_3/*g*-C_3N_4 hybrid and recycling test of α-Fe_2O_3/*g*-C_3N_4 (C). Reproduced from [170]. Copyright 2018, Wiley. (**b**) The photo-current response of the Nb-TiO_2, *g*-C_3N_4, and Nb-TiO_2/*g*-C_3N_4 under different excitation light conditions at an applied potential of 0 V (vs. NHE). Reproduced from [173]. Copyright 2019, Elsevier. (**c**) Schematic diagram of the photocatalytic process over face-to-face 2D/2D *g*-C_3N_4/$BiVO_4$ and proposed mechanism schematics of direct Z-scheme *g*-C_3N_4/$BiVO_4$ heterojunctions for photocatalytic CO_2 reduction. Reproduced from [92]. Copyright 2020, Elsevier. (**d**) Schematic diagram of the photocatalytic process over direct Z-scheme WO_3/*g*-C_3N_4 and stability analysis of WO_3/*g*-C_3N_4 for photocatalytic CO_2 reduction to CO and CH_4. Reproduced from [117]. Copyright 2020, Elsevier. (**e**) Schematic illustration of the preparation and CO_2 photoreduction process of the $Bi_{19}S_{27}Br_3$/*g*-C_3N_4 composite. Reproduced from [174]. Copyright 2022, Elsevier.

Table 3. Summary of direct Z-scheme photocatalysts based on *g*-C_3N_4 for CO_2 photoreduction.

Z-Scheme Photocatalyst	Fabrication	Irradiation Source	Products/Production (μmol g^{-1} h^{-1})/AQE	Reference
ZnO/*g*-C_3N_4	Solid-state	300 W simulated solar Xe arc lamp	CH_3OH: 0.6	[172]
SnO_{2-x}/*g*-C_3N_4	Solid-state	500 W Xe lamp	CO: ~19 CH_3OH: ~4 CH_4: ~2	[116]
g-C_3N_4/SnS_2	Hydrothermal method	300 W Xenon lamp ($\lambda \geq 420$ nm)	CH_3OH: 2.24 CO: 0.64	[91]
MoO_3/*g*-C_3N_4	impregnation method	350 W Xenon lamp (800 nm > λ > 420 nm)	CO: ~18 CH_3OH: ~7 CH_4: ~1	[85]

Table 3. *Cont.*

Z-Scheme Photocatalyst	Fabrication	Irradiation Source	Products/Production (μmol g^{-1} h^{-1})/AQE	Reference
α-Fe_2O_3/*g*-C_3N_4	Impregnation–hydrothermal method	Xenon lamp 0.21 Wcm^{-2}	CO: 27.2 AQE: 0.963% (420 nm)	[170]
AgCl/*g*-C_3N_4	Deposition-precipitation method	11 W fluorescent lamp	CH_4: ~2 CH_3COOH: ~0.75 HCOOH: ~0.31 AQE: 0.211% (475 nm)	[175]
$Cu_2V_2O_7$/*g*-C_3N_4	Calcination methodology	20 W white bulbs (700 nm > λ > 400 nm)	CH_4: 305 CO: 166 O_2: 706	[176]
g-C_3N_4/$FeWO_4$	Sonochemical method	300 W Xenon lamp (100 mW/cm^2)	CO: 6 AQE: ~0.3% (420 nm)	[83]
(Nb)TiO_2/*g*-C_3N_4	Calcination methodology	Two 30 W white bulbs	CH_4: 562 CO:420 HCOOH:698	[173]
2D/2D *g*-C_3N_4/$BiVO_4$	Hydrothermal method	300 W Xenon lamp (λ ≥ 420 nm)	CO: ~5.2 CH_4: ~4.6	[92]
$NiMoO_4$/*g*-C_3N_4	Calcined methodology	30 W LED, (700 nm > λ > 400 nm)	CH_4: 635 CO: 432 O_2: 1853 HCOOH: 647	[177]
α-Fe_2O_3/*g*-C_3N_4	Hydrothermal method	300 W xenon lamp	CO: 17.8 AQE: 0.31% (420 nm)	[178]
3D/2D WO_3/*g*-C_3N_4	Hydrothermal method	300 W Xenon lamp (100 mW cm^{-2})	CO: 145 CH_4: 133	[117]
$La_2Ti_2O_7$/*g*-C_3N_4	Ultrasonic-deposition method	Four blue LED (4 × 3 W, 420 nm)	CH_3OH: ~4 CO: ~2.5 AQE: 3.61% (420 nm)	[179]
Bi_2S_3/*g*-C_3N_4	Hydrothermal method	300 W xenon lamp	CO: 6.84 CH_4: 1.57 H_2: 1.38 AQE: 2.31% (420 nm)	[180]
ZnO/$ZnWO_4$/*g*-C_3N_4	Calcination method	Xenon lamp (300 W, 0.95 mW/cm^2)	CH_4: 6.2 CH_3OH: 3.8 CH_3CH_2OH: 2.1 CO: 1.3	[181]
$NiTiO_3$/*g*-C_3N_4	Ultrasonic-calcination method	300 W Xenon lamp (λ ≥ 420 nm)	CH_3OH: 13.74	[182]
$Bi_{19}S_{27}Br_3$/*g*-C_3N_4	Physical mixture (Strong grinding)	300 W xenon lamp	CO: 12.87	[174]

5. Conclusions and Outlook

In conclusion, *g*-C_3N_4-based direct Z-scheme photocatalysts are innovative alternatives for overcoming the main drawbacks of the parent material, i.e., high e^--h^+ recombination rate and inadequate redox potential. In this review, a comprehensive overview of the recent research on *g*-C_3N_4-based Z-scheme photocatalysts is described, focusing on the utilization of these systems in three environmental applications, such as pollutant abatement, H_2 evolution, and CO_2 reduction. There is undoubtedly a substantial amount of ground to cover by the scientific community since there are few reports where the synthesis and catalytic activity of novel *g*-C_3N_4-based direct Z-scheme photocatalysts have been studied. Especially, several synthetic methodologies (hydrothermal, solid-state, impregnation, etc.), characterization techniques to study the properties of Z-schemes (EPR, PL . . .), and the application of these materials in environmental reactions have been investigated, focusing on the effect of the catalysts and their catalytic activity to obtain efficient solar photocatalysts. Nevertheless, the photocatalytic efficiencies are still low, and many catalytic

mechanisms remain unclear. These characteristics represent the main drawbacks hindering the commercialization of these systems. The challenges for new researchers in the design and applicability of g-C_3N_4-based direct Z-scheme photocatalysts might be in the synthetic methodology of this photocatalyst, focusing on the interaction between g-C_3N_4 and another SC, since the intimate contact between both systems has a strong influence on the photocatalytic activity.

The effect of the dimensionality and surface chemistry of g-C_3N_4 and the hetero-counterpart present in the Z-scheme photocatalyst is a paradigm in heterostructure synthesis, and thus, in the improvement of the photocatalytic activity. Although the transfer directions of photogenerated charge carriers in Z-scheme systems are studied by EPR, photoluminescence spectroscopy, reactive species scavenging experiments, and theoretical calculations, it is necessary to develop more powerful characterization tools to investigate the charge-transfer mechanism. Subsequently, it is also mandatory to understand the electron photoexcitation, trapping, and migration at the interface through a series of *operando* characterization techniques and computational studies.

Regarding the applicability of Z-schemes in environmental reactions, it is essential to develop new techniques to elucidate the mechanisms of catalytic reactions in all the stages of these catalytic processes (adsorption, reaction, and desorption), considering that the monitoring of the reaction is sometimes complex due to the formation of by-products. This scenario opens the door for the design and engineering of new Z-schemes based on g-C_3N_4, and the development of characterization techniques and studies of new mechanisms to obtain active photocatalysts in environmental applications under visible light.

Author Contributions: Conceptualization, J.F.-C., R.G., M.N.-G., Á.B.-M. and D.C.-A.; writing—original draft preparation, J.F.-C. and R.G.; writing—review and editing R.G., M.N.-G., W.C., Á.B.-M. and D.C.-A.; supervision, M.N.-G., W.C., Á.B.-M. and D.C.-A. All authors have read and agreed to the published version of the manuscript.

Funding: This research was funded by European Union-Next Generation EU, MINECO, and University of Alicante: MARSALAS21-09, Generalitat Valenciana: CDEIGENT/2018/027, University of Alicante: GRE20-19-A. PID2021-123079OB-I00 project funded by MCIN/AEI/10.13039/501100011033 and "ERDF A way of making Europe", European Union's Horizon 2020 research and innovation programme: Grant Agreement 101002219 and Generalitat Valenciana: Proyecto Prometeo CIPROM/2021/70.

Data Availability Statement: Not applicable.

Acknowledgments: J.F.-C. thanks European Union-Next Generation EU, MINECO, and University of Alicante for a postdoctoral researcher grant (MARSALAS21-09). M.N.-G. would like to thank the Plan GenT project from Generalitat Valenciana (CDEIGENT/2018/027), and the Vicerrectorado de Investigación y Transferencia de Conocimiento de la Universidad de Alicante (GRE20-19-A) for the financial support. PID2021-123079OB-I00 project funded by MCIN/AEI/10.13039/501100011033 and "ERDF A way of making Europe", European Research Council (ERC) under the European Union's Horizon 2020 research and innovation programme (Grant Agreement 101002219), and Generalitat Valenciana (Proyecto Prometeo CIPROM/2021/70) are also acknowledged.

Conflicts of Interest: The authors declare no conflict of interest.

References

1. Toman, M.A.; Morgenstern, R.D.; Anderson, J. The Economics of "When" Flexibility in the Design of Greenhouse Gas Abatement Policies. *Annu. Rev. Environ. Resour.* **1999**, *24*, 431–460.
2. Vijayavenkataraman, S.; Iniyan, S.; Goic, R. A Review of Climate Change, Mitigation and Adaptation. *Renew. Sustain. Energy Rev.* **2012**, *16*, 878–897. [CrossRef]
3. Manisalidis, I.; Stavropoulou, E.; Stavropoulos, A.; Bezirtzoglou, E. Environmental and Health Impacts of Air Pollution: A Review. *Front. Public Health* **2020**, *8*, 14. [CrossRef]
4. Paltsev, S. Energy Scenarios: The Value and Limits of Scenario Analysis. *Wiley Interdiscip. Rev. Energy Environ.* **2017**, *6*, 1–19. [CrossRef]
5. Solangi, K.H.; Islam, M.R.; Saidur, R.; Rahim, N.A.; Fayaz, H. A Review on Global Solar Energy Policy. *Renew. Sustain. Energy Rev.* **2011**, *15*, 2149–2163. [CrossRef]

6. Kannan, N.; Vakeesan, D. Solar Energy for Future World—A Review. *Renew. Sustain. Energy Rev.* **2016**, *62*, 1092–1105. [CrossRef]
7. Kabir, E.; Kumar, P.; Kumar, S.; Adelodun, A.A.; Kim, K.H. Solar Energy: Potential and Future Prospects. *Renew. Sustain. Energy Rev.* **2018**, *82*, 894–900. [CrossRef]
8. Alharbi, N.S.; Hu, B.; Hayat, T.; Rabah, S.O.; Alsaedi, A.; Zhuang, L.; Wang, X. Efficient Elimination of Environmental Pollutants through Sorption-Reduction and Photocatalytic Degradation Using Nanomaterials. *Front. Chem. Sci. Eng.* **2020**, *14*, 1124–1135. [CrossRef]
9. Saravanan, A.; Senthil Kumar, P.; Vo, D.V.N.; Jeevanantham, S.; Bhuvaneswari, V.; Anantha Narayanan, V.; Yaashikaa, P.R.; Swetha, S.; Reshma, B. A Comprehensive Review on Different Approaches for CO_2 Utilization and Conversion Pathways. *Chem. Eng. Sci.* **2021**, *236*, 116515. [CrossRef]
10. Melchionna, M.; Fornasiero, P. Updates on the Roadmap for Photocatalysis. *ACS Catal.* **2020**, *10*, 5493–5501. [CrossRef]
11. Long, Z.; Li, Q.; Wei, T.; Zhang, G.; Ren, Z. Historical Development and Prospects of Photocatalysts for Pollutant Removal in Water. *J. Hazard. Mater.* **2020**, *395*, 122599. [CrossRef]
12. Maeda, K.; Domen, K. Photocatalytic Water Splitting: Recent Progress and Future Challenges. *J. Phys. Chem. Lett.* **2010**, *1*, 2655–2661. [CrossRef]
13. Nishiyama, H.; Yamada, T.; Nakabayashi, M.; Maehara, Y.; Yamaguchi, M.; Kuromiya, Y.; Nagatsuma, Y.; Tokudome, H.; Akiyama, S.; Watanabe, T.; et al. Photocatalytic Solar Hydrogen Production from Water on a 100-M^2 Scale. *Nature* **2021**, *598*, 304–307. [CrossRef] [PubMed]
14. Tuller, H.L. Solar to Fuels Conversion Technologies: A Perspective. *Mater. Renew. Sustain. Energy* **2017**, *6*, 3. [CrossRef] [PubMed]
15. Fujishima, A.; Honda, K. Electrochemical Photolysis of Water at a Semiconductor Electrode. *Nature* **1972**, *238*, 37–38. [CrossRef] [PubMed]
16. Nakata, K.; Fujishima, A. TiO_2 Photocatalysis: Design and Applications. *J. Photochem. Photobiol. C Photochem. Rev.* **2012**, *13*, 169–189. [CrossRef]
17. Wenderich, K.; Mul, G. Methods, Mechanism, and Applications of Photodeposition in Photocatalysis: A Review. *Chem. Rev.* **2016**, *116*, 14587–14619. [CrossRef]
18. Schneider, J.; Matsuoka, M.; Takeuchi, M.; Zhang, J.; Horiuchi, Y.; Anpo, M.; Bahnemann, D.W. Understanding TiO_2 Photocatalysis Mechanisms and Materials. *Chem. Rev.* **2014**, *114*, 9919–9986.
19. He, R.; Cao, S.; Zhou, P.; Yu, J. Recent Advances in Visible Light Bi-Based Photocatalysts. *Chin. J. Catal.* **2014**, *35*, 989–1007. [CrossRef]
20. Han, G.; Sun, Y. Visible-Light-Driven Organic Transformations on Semiconductors. *Mater. Today Phys.* **2021**, *16*, 100297. [CrossRef]
21. Wen, J.; Xie, J.; Chen, X.; Li, X. A Review on G-C_3N_4-Based Photocatalysts. *Appl. Surf. Sci.* **2017**, *391*, 72–123. [CrossRef]
22. Hayat, A.; Al-Sehemi, A.G.; El-Nasser, K.S.; Taha, T.A.; Al-Ghamdi, A.A.; Shah Syed, J.A.; Amin, M.A.; Ali, T.; Bashir, T.; Palamanit, A.; et al. Graphitic Carbon Nitride (g–C_3N_4)–Based Semiconductor as a Beneficial Candidate in Photocatalysis Diversity. *Int. J. Hydrogen Energy* **2022**, *47*, 5142–5191. [CrossRef]
23. Gan, X.; Lei, D.; Wong, K.Y. Two-Dimensional Layered Nanomaterials for Visible-Light-Driven Photocatalytic Water Splitting. *Mater. Today Energy* **2018**, *10*, 352–367. [CrossRef]
24. Ismael, M. A Review on Graphitic Carbon Nitride (g-C_3N_4) Based Nanocomposites: Synthesis, Categories, and Their Application in Photocatalysis. *J. Alloys Compd.* **2020**, *846*, 156446. [CrossRef]
25. Huang, D.; Li, Z.; Zeng, G.; Zhou, C.; Xue, W.; Gong, X.; Yan, X.; Chen, S.; Wang, W.; Cheng, M. Megamerger in Photocatalytic Field: 2D g-C_3N_4 Nanosheets Serve as Support of 0D Nanomaterials for Improving Photocatalytic Performance. *Appl. Catal. B Environ.* **2019**, *240*, 153–173. [CrossRef]
26. Fu, J.; Yu, J.; Jiang, C.; Cheng, B. G-C_3N_4-Based Heterostructured Photocatalysts. *Adv. Energy Mater.* **2018**, *8*, 1701503. [CrossRef]
27. Li, Y.; Zhou, M.; Cheng, B.; Shao, Y. Recent Advances in G-C_3N_4-Based Heterojunction Photocatalysts. *J. Mater. Sci. Technol.* **2020**, *56*, 1–17. [CrossRef]
28. Liao, G.; Li, C.; Li, X.; Fang, B. Emerging Polymeric Carbon Nitride Z-Scheme Systems for Photocatalysis. *Cell Rep. Phys. Sci.* **2021**, *2*, 100355. [CrossRef]
29. Belousov, A.S.; Fukina, D.G.; Koryagin, A.V. Metal–organic framework-basedheterojunction photocatalysts for organicpollutant degradation: Design, construction, and performances. *J. Chem. Technol. Biotechnol.* **2022**, *97*, 2675–2693. [CrossRef]
30. Zhao, Y.; Linghu, X.; Shu, Y.; Zhang, J.; Chen, Z.; Wu, Y.; Shan, D.; Wang, B. Classification and Catalytic Mechanisms of Heterojunction Photocatalysts and the Application of Titanium Dioxide (TiO_2)-Based Heterojunctions in Environmental Remediation. *J. Environ. Chem. Eng.* **2022**, *10*, 108077. [CrossRef]
31. Low, J.; Yu, J.; Jaroniec, M.; Wageh, S.; Al-Ghamdi, A.A. Heterojunction Photocatalysts. *Adv. Mater.* **2017**, *29*, 1601694. [CrossRef] [PubMed]
32. Liao, G.; Li, C.; Liu, S.Y.; Fang, B.; Yang, H. Emerging Frontiers of Z-Scheme Photocatalytic Systems. *Trends Chem.* **2022**, *4*, 111–127. [CrossRef]
33. Ghosh, U.; Pal, A. Graphitic Carbon Nitride Based Z Scheme Photocatalysts: Design Considerations, Synthesis, Characterization and Applications. *J. Ind. Eng. Chem.* **2019**, *79*, 383–408. [CrossRef]
34. Zhang, W.; Mohamed, A.R.; Ong, W.J. Z-Scheme Photocatalytic Systems for Carbon Dioxide Reduction: Where Are We Now? *Angew. Chem.-Int. Ed.* **2020**, *59*, 22894–22915. [CrossRef] [PubMed]

35. Yuan, Y.; Guo, R.T.; Hong, L.F.; Ji, X.Y.; Lin, Z.D.; Li, Z.S.; Pan, W.G. A Review of Metal Oxide-Based Z-Scheme Heterojunction Photocatalysts: Actualities and Developments. *Mater. Today Energy* **2021**, *21*, 100829. [CrossRef]
36. Low, J.; Jiang, C.; Cheng, B.; Wageh, S.; Al-Ghamdi, A.A.; Yu, J. A Review of Direct Z-Scheme Photocatalysts. *Small Methods* **2017**, *1*, 1700080. [CrossRef]
37. Li, X.; Garlisi, C.; Guan, Q.; Anwer, S.; Al-Ali, K.; Palmisano, G.; Zheng, L. A Review of Material Aspects in Developing Direct Z-Scheme Photocatalysts. *Mater. Today* **2021**, *47*, 75–107. [CrossRef]
38. Zhang, H.; Tian, W.; Zhang, J.; Duan, X.; Liu, S.; Sun, H.; Wang, S. Carbon Nitride-Based Z-Scheme Photocatalysts for Non-Sacrificial Overall Water Splitting. *Mater. Today Energy* **2022**, *23*, 100915. [CrossRef]
39. Lin, J.; Tian, W.; Zhang, H.; Duan, X.; Sun, H.; Wang, S. Graphitic Carbon Nitride-Based Z-Scheme Structure for Photocatalytic CO_2 Reduction. *Energy Fuels* **2021**, *35*, 7–24. [CrossRef]
40. Kumar, Y.; Kumar, R.; Raizada, P.; Aslam, A.; Van Le, Q.; Singh, P.; Nguyen, V.-H. Novel Z-Scheme $ZnIn_2S_4$-based photocatalysts for solar-driven environmental and energy applications: Progress and perspectives. *J. Mater. Sci. Technol.* **2021**, *87*, 234–257. [CrossRef]
41. Li, Y.; Pan, C.; Wang, G.; Leng, Y.; Jiang, P.; Dong, Y.; Zhu, Y. Improving the photocatalytic activity of benzyl alcohol oxidation by Z-scheme SnS/g-C3N4. *New J. Chem.* **2021**, *45*, 6611–6617. [CrossRef]
42. Ma, X.; Huo, X.; Hao, K.; Song, L.; Yu, Q.; Liu, T.; Wang, Z. Visible Light Driven VO_2/g-C_3N_4 Z-Scheme Composite Photocatalysts for Selective Oxidation of DL-1-Phenylethyl Alcohol under Vis-LEDs Irradiation and Aerobic Oxidation. *Chem. Select* **2021**, *6*, 2101–2211.
43. Belousov, A.; Suleimanov, E.V. Application of metal–organic frameworks as an alternative to metal oxide-based photocatalysts for the production of industrially important organic chemicals. *Green Chem.* **2021**, *23*, 6172–6204. [CrossRef]
44. Ma, J.; Yang, X.; Yao, S.; Guo, Y.; Sun, S. Photocatalytic Biorefinery to Lactic Acid: A Carbon Nitride Framework with O Atoms Replacing the Graphitic N Linkers Shows Fast Migration/Separation of Charge. *ChemCatChem* **2022**, *14*, e2022000. [CrossRef]
45. Rono, N.; Kibet, J.K.; Martincigh, B.S.; Nyamori, V.O. A Review of the Current Status of Graphitic Carbon Nitride. *Crit. Rev. Solid State Mater. Sci.* **2021**, *46*, 189–217. [CrossRef]
46. Inagaki, M.; Tsumura, T.; Kinumoto, T.; Toyoda, M. Graphitic Carbon Nitrides (g-C_3N_4) with Comparative Discussion to Carbon Materials. *Carbon* **2019**, *141*, 580–607. [CrossRef]
47. Ong, W.J.; Tan, L.L.; Ng, Y.H.; Yong, S.T.; Chai, S.P. Graphitic Carbon Nitride (g-C_3N_4)-Based Photocatalysts for Artificial Photosynthesis and Environmental Remediation: Are We a Step Closer to Achieving Sustainability? *Chem. Rev.* **2016**, *116*, 7159–7329. [CrossRef]
48. Wang, J.; Wang, S. A Critical Review on Graphitic Carbon Nitride (g-C_3N_4)-Based Materials: Preparation, Modification and Environmental Application. *Coord. Chem. Rev.* **2022**, *453*, 214338. [CrossRef]
49. Kroke, E.; Schwarz, M. Novel Group 14 Nitrides. *Coord. Chem. Rev.* **2004**, *248*, 493–532. [CrossRef]
50. Alaghmandfard, A.; Ghandi, K. A Comprehensive Review of Graphitic Carbon Nitride (g-C_3N_4)–Metal Oxide-Based Nanocomposites: Potential for Photocatalysis and Sensing. *Nanomaterials* **2022**, *12*, 294. [CrossRef]
51. Liu, N.; Li, T.; Zhao, Z.; Liu, J.; Luo, X.; Yuan, X.; Luo, K.; Luo, K.; He, J.; Yu, D.; et al. From Triazine to Heptazine: Origin of Graphitic Carbon Nitride as a Photocatalyst. *ACS Omega* **2020**, *5*, 12557–12567. [CrossRef] [PubMed]
52. Wang, X.; Blechert, S.; Antonietti, M. Polymeric Graphitic Carbon Nitride for Heterogeneous Photocatalysis. *ACS Catal.* **2012**, *2*, 1596–1606. [CrossRef]
53. Ismael, M.; Wu, Y. A Mini-Review on the Synthesis and Structural Modification of g-C_3N_4-Based Materials, and Their Applications in Solar Energy Conversion and Environmental Remediation. *Sustain. Energy Fuels* **2019**, *3*, 2907–2925. [CrossRef]
54. Papailias, I.; Giannakopoulou, T.; Todorova, N.; Demotikali, D.; Vaimakis, T.; Trapalis, C. Effect of Processing Temperature on Structure and Photocatalytic Properties of G-C_3N_4. *Appl. Surf. Sci.* **2015**, *358*, 278–286. [CrossRef]
55. Nguyen, T.K.A.; Pham, T.T.; Nguyen-Phu, H.; Shin, E.W. The Effect of Graphitic Carbon Nitride Precursors on the Photocatalytic Dye Degradation of Water-Dispersible Graphitic Carbon Nitride Photocatalysts. *Appl. Surf. Sci.* **2021**, *537*, 148027. [CrossRef]
56. Wang, X.; Maeda, K.; Thomas, A.; Takanabe, K.; Xin, G.; Carlsson, J.M.; Domen, K.; Antonietti, M. A Metal-Free Polymeric Photocatalyst for Hydrogen Production from Water under Visible Light. *Nat. Mater.* **2009**, *8*, 76–80. [CrossRef]
57. Aslam, I.; Hassan Farooq, M.; Ghani, U.; Rizwan, M.; Nabi, G.; Shahzad, W.; Boddula, R. Synthesis of Novel G-C_3N_4 Microrods: A Metal-Free Visible-Light-Driven Photocatalyst. *Mater. Sci. Energy Technol.* **2019**, *2*, 401–407. [CrossRef]
58. Wu, X.; Liu, C.; Li, X.; Zhang, X.; Wang, C.; Liu, Y. Effect of Morphology on the Photocatalytic Activity of G-C_3N_4 Photocatalysts under Visible-Light Irradiation. *Mater. Sci. Semicond. Process.* **2015**, *32*, 76–81. [CrossRef]
59. Ren, Y.; Zeng, D.; Ong, W.J. Interfacial Engineering of Graphitic Carbon Nitride (g-C_3N_4)-Based Metal Sulfide Heterojunction Photocatalysts for Energy Conversion: A Review. *Chin. J. Catal.* **2019**, *40*, 289–319. [CrossRef]
60. Zhu, B.; Cheng, B.; Fan, J.; Ho, W.; Yu, J. G-C_3N_4-Based 2D/2D Composite Heterojunction Photocatalyst. *Small Struct.* **2021**, *2*, 2100086. [CrossRef]
61. Wang, Y.; Suzuki, H.; Xie, J.; Tomita, O.; Martin, D.J.; Higashi, M.; Kong, D.; Abe, R.; Tang, J. Mimicking Natural Photosynthesis: Solar to Renewable H_2 Fuel Synthesis by Z-Scheme Water Splitting Systems. *Chem. Rev.* **2018**, *118*, 5201–5241. [CrossRef] [PubMed]
62. Huang, D.; Chen, S.; Zeng, G.; Gong, X.; Zhou, C.; Cheng, M.; Xue, W.; Yan, X.; Li, J. Artificial Z-Scheme Photocatalytic System: What Have Been Done and Where to Go? *Coord. Chem. Rev.* **2019**, *385*, 44–80. [CrossRef]

63. Bard, A.J. Photoelectrochemistry and Heterogeneous Photo-Catalysis at Semiconductors. *J. Photochem.* **1979**, *10*, 59–75. [CrossRef]
64. Tada, H.; Mitsui, T.; Kiyonaga, T.; Akita, T.; Tanaka, K. All-Solid-State Z-Scheme in CdS-Au-TiO_2 Three-Component Nanojunction System. *Nat. Mater.* **2006**, *5*, 782–786. [CrossRef] [PubMed]
65. Sharma, S.; Dutta, V.; Raizada, P.; Khan, A.A.P.; Van Le, Q.; Thakur, V.K.; Biswas, J.K.; Selvasembian, R.; Singh, P. Controllable Functionalization of G-C_3N_4 Mediated All-Solid-State (ASS) Z-Scheme Photocatalysts towards Sustainable Energy and Environmental Applications. *Environ. Technol. Innov.* **2021**, *24*, 101972. [CrossRef]
66. Yu, J.; Wang, S.; Low, J.; Xiao, W. Enhanced Photocatalytic Performance of Direct Z-Scheme g-C_3N_4-TiO_2 Photocatalysts for the Decomposition of Formaldehyde in Air. *Phys. Chem. Chem. Phys.* **2013**, *15*, 16883–16890. [CrossRef] [PubMed]
67. Lin, J.; Tian, W.; Zhang, H.; Duan, X.; Sun, H.; Wang, H.; Fang, Y.; Huang, Y.; Wang, S. Carbon Nitride-Based Z-Scheme Heterojunctions for Solar-Driven Advanced Oxidation Processes. *J. Hazard. Mater.* **2022**, *434*, 128866. [CrossRef]
68. Zhao, D.; Guan, X.; Shen, S. Design of Polymeric Carbon Nitride-Based Heterojunctions for Photocatalytic Water Splitting: A Review. *Environ. Chem. Lett.* **2022**, *7*, 1–19. [CrossRef]
69. Xu, Q.; Zhang, L.; Yu, J.; Wageh, S.; Al-Ghamdi, A.A.; Jaroniec, M. Direct Z-Scheme Photocatalysts: Principles, Synthesis, and Applications. *Mater. Today* **2018**, *21*, 1042–1063. [CrossRef]
70. Zhang, Y.; Liu, J.; Wu, G.; Chen, W. Porous Graphitic Carbon Nitride Synthesized via Direct Polymerization of Urea for Efficient Sunlight-Driven Photocatalytic Hydrogen Production. *Nanoscale* **2012**, *4*, 5300–5303. [CrossRef]
71. Kumar, S.; Karthikeyan, S.; Lee, A.F. G-C_3N_4-Based Nanomaterials for Visible Light-Driven Photocatalysis. *Catalysts* **2018**, *8*, 74. [CrossRef]
72. Wiley, J.B.; Kaner, R.B. Rapid Solid-State Precursor Synthesis of Materials. *Science* **1992**, *255*, 1093–1097. [CrossRef] [PubMed]
73. Stein, A.; Keller, S.W.; Mallouk, T.E. Turning down the Heat: Design and Mechanism in Solid-State Synthesis. *Science* **1993**, *259*, 1558–1564. [CrossRef] [PubMed]
74. Lu, L.; Wang, G.; Zou, M.; Wang, J.; Li, J. Effects of Calcining Temperature on Formation of Hierarchical TiO_2/g-C $_3N_4$ Hybrids as an Effective Z-Scheme Heterojunction Photocatalyst. *Appl. Surf. Sci.* **2018**, *441*, 1012–1023. [CrossRef]
75. Yu, W.; Chen, J.; Shang, T.; Chen, L.; Gu, L.; Peng, T. Direct Z-Scheme g-C_3N_4/WO_3 Photocatalyst with Atomically Defined Junction for H_2 Production. *Appl. Catal. B Environ.* **2017**, *219*, 693–704. [CrossRef]
76. Chrouda, A.; Mahmoud Ali Ahmed, S.; Babiker Elamin, M. Preparation of Nanocatalysts Using Deposition Precipitation with Urea: Mechanism, Advantages and Results. *ChemBioEng Rev.* **2022**, *9*, 248–264. [CrossRef]
77. Wen, X.J.; Shen, C.H.; Fei, Z.H.; Fang, D.; Liu, Z.T.; Dai, J.T.; Niu, C.G. Recent Developments on AgI Based Heterojunction Photocatalytic Systems in Photocatalytic Application. *Chem. Eng. J.* **2020**, *383*, 123083. [CrossRef]
78. Gupta, B.; Melvin, A.A.; Matthews, T.; Dash, S.; Tyagi, A.K. TiO_2 Modification by Gold (Au) for Photocatalytic Hydrogen (H_2) Production. *Renew. Sustain. Energy Rev.* **2016**, *58*, 1366–1375. [CrossRef]
79. Olivares, F.; Peón, F.; Henríquez, R.; del Río, R.S. Strategies for Area-Selective Deposition of Metal Nanoparticles on Carbon Nanotubes and Their Applications: A Review. *J. Mater. Sci.* **2022**, *57*, 2362–2387. [CrossRef]
80. Guo, W.; Fan, K.; Zhang, J.; Xu, C. 2D/2D Z-Scheme Bi_2WO_6/Porous-g-C_3N_4 with Synergy of Adsorption and Visible-Light-Driven Photodegradation. *Appl. Surf. Sci.* **2018**, *447*, 125–134. [CrossRef]
81. Hutchings, G.J.; Kiely, C.J. Strategies for the Synthesis of Supported Gold Palladium Nanoparticles with Controlled Morphology and Composition. *Acc. Chem. Res.* **2013**, *46*, 1759–1772. [CrossRef] [PubMed]
82. Campanati, M.; Fornasari, G.; Vaccari, A. Fundamentals in the Preparation of Heterogeneous Catalysts. *Catal. Today* **2003**, *77*, 299–314. [CrossRef]
83. Bhosale, R.; Jain, S.; Vinod, C.P.; Kumar, S.; Ogale, S. Direct Z-Scheme g-C_3N_4/$FeWO_4$ Nanocomposite for Enhanced and Selective Photocatalytic CO_2 Reduction under Visible Light. *ACS Appl. Mater. Interfaces* **2019**, *11*, 6174–6183. [CrossRef]
84. Jin, Z.; Hu, R.; Wang, H.; Hu, J.; Ren, T. One-Step Impregnation Method to Prepare Direct Z-Scheme $LaCoO_3$/g-C_3N_4 Heterojunction Photocatalysts for Phenol Degradation under Visible Light. *Appl. Surf. Sci.* **2019**, *491*, 432–442. [CrossRef]
85. Feng, Z.; Zeng, L.; Chen, Y.; Ma, Y.; Zhao, C.; Jin, R.; Lu, Y.; Wu, Y.; He, Y. In Situ Preparation of Z-Scheme MoO_3/g-C_3N_4 Composite with High Performance in Photocatalytic CO_2 Reduction and RhB Degradation. *J. Mater. Res.* **2017**, *32*, 3660–3668. [CrossRef]
86. Zhou, D.; Yu, B.; Chen, Q.; Shi, H.; Zhang, Y.; Li, D.; Yang, X.; Zhao, W.; Liu, C.; Wei, G.; et al. Improved Visible Light Photocatalytic Activity on Z-Scheme g-C_3N_4 Decorated TiO_2 Nanotube Arrays by a Simple Impregnation Method. *Mater. Res. Bull.* **2020**, *124*, 110757. [CrossRef]
87. Darr, J.A.; Zhang, J.; Makwana, N.M.; Weng, X. Continuous Hydrothermal Synthesis of Inorganic Nanoparticles: Applications and Future Directions. *Chem. Rev.* **2017**, *117*, 11125–11238. [CrossRef]
88. Kaya, C.; He, J.Y.; Gu, X.; Butler, E.G. Nanostructured Ceramic Powders by Hydrothermal Synthesis and Their Applications. *Microporous Mesoporous Mater.* **2002**, *54*, 37–49. [CrossRef]
89. Byrappa, K.; Adschiri, T. Hydrothermal Technology for Nanotechnology. *Prog. Cryst. Growth Charact. Mater.* **2007**, *53*, 117–166. [CrossRef]
90. Jo, W.K.; Natarajan, T.S. Influence of TiO_2 Morphology on the Photocatalytic Efficiency of Direct Z-Scheme g-C_3N_4/TiO_2 Photocatalysts for Isoniazid Degradation. *Chem. Eng. J.* **2015**, *281*, 549–565. [CrossRef]
91. Di, T.; Zhu, B.; Cheng, B.; Yu, J.; Xu, J. A Direct Z-Scheme g-C_3N_4/SnS_2 Photocatalyst with Superior Visible-Light CO_2 Reduction Performance. *J. Catal.* **2017**, *352*, 532–541. [CrossRef]

92. Lu, M.; Li, Q.; Zhang, C.; Fan, X.; Li, L.; Dong, Y.; Chen, G.; Shi, H. Remarkable Photocatalytic Activity Enhancement of CO_2 Conversion over 2D/2D g-C_3N_4/$BiVO_4$ Z-Scheme Heterojunction Promoted by Efficient Interfacial Charge Transfer. *Carbon* **2020**, *160*, 342–352. [CrossRef]
93. Wu, Y.; Zhao, X.; Huang, S.; Li, Y.; Zhang, X.; Zeng, G.; Niu, L.; Ling, Y.; Zhang, Y. Facile Construction of 2D G-C_3N_4 Supported Nanoflower-like $NaBiO_3$ with Direct Z-Scheme Heterojunctions and Insight into Its Photocatalytic Degradation of Tetracycline. *J. Hazard. Mater.* **2021**, *414*, 125547. [CrossRef]
94. Lakshmanareddy, N.; Navakoteswara Rao, V.; Cheralathan, K.K.; Subramaniam, E.P.; Shankar, M.V. Pt/TiO_2 Nanotube Photocatalyst–Effect of Synthesis Methods on Valance State of Pt and Its Influence on Hydrogen Production and Dye Degradation. *J. Colloid Interface Sci.* **2019**, *538*, 83–98. [CrossRef]
95. Magdziarz, A.; Colmenares, J.C. In Situ Coupling of Ultrasound to Electro-and Photo-Deposition Methods for Materials Synthesis. *Molecules* **2017**, *22*, 216. [CrossRef] [PubMed]
96. Jiang, W.; Qu, D.; An, L.; Gao, X.; Wen, Y.; Wang, X.; Sun, Z. Deliberate Construction of Direct Z -Scheme Photocatalysts through Photodeposition. *J. Mater. Chem. A* **2019**, *7*, 18348–18356. [CrossRef]
97. Sari, F.N.I.; Yen, D.T.K.; Ting, J.M. Enhanced Photocatalytic Performance of TiO_2 through a Novel Direct Dual Z-Scheme Design. *Appl. Surf. Sci.* **2020**, *533*, 147506. [CrossRef]
98. Rhimi, B.; Wang, C.; Bahnemann, D.W. Latest Progress in G-C_3N_4 Based Heterojunctions for Hydrogen Production via Photocatalytic Water Splitting: A Mini Review. *J. Phys. Energy* **2020**, *2*, 042003. [CrossRef]
99. Pourshirband, N.; Nezamzadeh-Ejhieh, A. An Efficient Z-Scheme CdS/g-C_3N_4 Nano Catalyst in Methyl Orange Photodegradation: Focus on the Scavenging Agent and Mechanism. *J. Mol. Liq.* **2021**, *335*, 116543. [CrossRef]
100. Chiu, Y.H.; Chang, T.F.M.; Chen, C.Y.; Sone, M.; Hsu, Y.J. Mechanistic Insights into Photodegradation of Organic Dyes Using Heterostructure Photocatalysts. *Catalysts* **2019**, *9*, 430. [CrossRef]
101. Bai, Y.; Wang, P.Q.; Liu, J.Y.; Liu, X.J. Enhanced Photocatalytic Performance of Direct Z-Scheme BiOCl-g-C_3N_4 Photocatalysts. *RSC Adv.* **2014**, *4*, 19456–19461. [CrossRef]
102. Jiang, W.; Zong, X.; An, L.; Hua, S.; Miao, X.; Luan, S.; Wen, Y.; Tao, F.F.; Sun, Z. Consciously Constructing Heterojunction or Direct Z-Scheme Photocatalysts by Regulating Electron Flow Direction. *ACS Catal.* **2018**, *8*, 2209–2217. [CrossRef]
103. Zhang, J.; Hu, Y.; Jiang, X.; Chen, S.; Meng, S.; Fu, X. Design of a Direct Z-Scheme Photocatalyst: Preparation and Characterization of Bi_2O_3/g-C_3N_4 with High Visible Light Activity. *J. Hazard. Mater.* **2014**, *280*, 713–722. [CrossRef] [PubMed]
104. Low, J.; Dai, B.; Tong, T.; Jiang, C.; Yu, J. In Situ Irradiated X-Ray Photoelectron Spectroscopy Investigation on a Direct Z-Scheme TiO_2/CdS Composite Film Photocatalyst. *Adv. Mater.* **2019**, *31*, 1802981. [CrossRef]
105. Han, Q.; Li, L.; Gao, W.; Shen, Y.; Wang, L.; Zhang, Y.; Wang, X.; Shen, Q.; Xiong, Y.; Zhou, Y.; et al. Elegant Construction of $ZnIn_2S_4$/$BiVO_4$ Hierarchical Heterostructures as Direct Z-Scheme Photocatalysts for Efficient CO_2 Photoreduction. *ACS Appl. Mater. Interfaces* **2021**, *13*, 15092–15100. [CrossRef]
106. Zhou, Z.; Niu, X.; Zhang, Y.; Wang, J. Janus MoSSe/WSeTe Heterostructures: A Direct Z-Scheme Photocatalyst for Hydrogen Evolution. *J. Mater. Chem. A* **2019**, *7*, 21835–21842. [CrossRef]
107. Abdul Nasir, J.; Munir, A.; Ahmad, N.; Haq, T.U.; Khan, Z.; Rehman, Z. Photocatalytic Z-Scheme Overall Water Splitting: Recent Advances in Theory and Experiments. *Adv. Mater.* **2021**, *33*, 105195. [CrossRef]
108. Lu, Q.; Eid, K.; Li, W.; Abdullah, A.M.; Xu, G.; Varma, R.S. Engineering Graphitic Carbon Nitride (g-C_3N_4) for Catalytic Reduction of CO_2 to Fuels and Chemicals: Strategy and Mechanism. *Green Chem.* **2021**, *23*, 5394–5428. [CrossRef]
109. Saravanan, A.; Kumar, P.S.; Vo, D.V.N.; Yaashikaa, P.R.; Karishma, S.; Jeevanantham, S.; Gayathri, B.; Bharathi, V.D. Photocatalysis for Removal of Environmental Pollutants and Fuel Production: A Review. *Environ. Chem. Lett.* **2021**, *19*, 441–463. [CrossRef]
110. Yu, X.; Ng, S.F.; Putri, L.K.; Tan, L.L.; Mohamed, A.R.; Ong, W.J. Point-Defect Engineering: Leveraging Imperfections in Graphitic Carbon Nitride (g-C_3N_4) Photocatalysts toward Artificial Photosynthesis. *Small* **2021**, *17*, 2006851. [CrossRef]
111. Fu, Y.; Li, Z.; Liu, Q.; Yang, X.; Tang, H. Construction of Carbon Nitride and MoS_2 Quantum Dot 2D/0D Hybrid Photocatalyst: Direct Z-Scheme Mechanism for Improved Photocatalytic Activity. *Chin. J. Catal.* **2017**, *38*, 2160–2170. [CrossRef]
112. Jing, L.; Xu, Y.; Liu, J.; Zhou, M.; Xu, H.; Xie, M.; Li, H.; Xie, J. Direct Z-Scheme Red Carbon Nitride/Rod-like Lanthanum Vanadate Composites with Enhanced Photodegradation of Antibiotic Contaminants. *Appl. Catal. B Environ.* **2020**, *277*, 119245. [CrossRef]
113. Zhou, D.; Chen, Z.; Yang, Q.; Shen, C.; Tang, G.; Zhao, S.; Zhang, J.; Chen, D.; Wei, Q.; Dong, X. Facile Construction of G-C_3N_4 Nanosheets/TiO_2 Nanotube Arrays as Z-Scheme Photocatalyst with Enhanced Visible-Light Performance. *ChemCatChem* **2016**, *8*, 3064–3073. [CrossRef]
114. Yang, Y.; Chen, J.; Liu, C.; Sun, Z.; Qiu, M.; Yan, G.; Gao, F. Dual-Z-Scheme Heterojunction for Facilitating Spacial Charge Transport Toward Ultra-Efficient Photocatalytic H_2 Production. *Sol. RRL* **2021**, *5*, 2100241. [CrossRef]
115. Idrees, F.; Dillert, R.; Bahnemann, D.; Butt, F.K.; Tahir, M. In-Situ Synthesis of Nb_2O_5/g-C_3N_4 Heterostructures as Highly Efficient Photocatalysts for Molecular H_2 Evolution under Solar Illumination. *Catalysts* **2019**, *9*, 169. [CrossRef]
116. He, Y.; Zhang, L.; Fan, M.; Wang, X.; Walbridge, M.L.; Nong, Q.; Wu, Y.; Zhao, L. Z-Scheme SnO_2-x/g-C_3N_4 Composite as an Efficient Photocatalyst for Dye Degradation and Photocatalytic CO_2 Reduction. *Sol. Energy Mater. Sol. Cells* **2015**, *137*, 175–184. [CrossRef]
117. Tahir, B.; Tahir, M.; Mohd Nawawi, M.G. Highly STable 3D/2D WO_3/g-C_3N_4 Z-Scheme Heterojunction for Stimulating Photocatalytic CO_2 Reduction by H_2O/H_2 to CO and CH_4 under Visible Light. *J. CO_2 Util.* **2020**, *41*, 101270. [CrossRef]

118. Deng, Y.; Zhao, R. Advanced Oxidation Processes (AOPs) in Wastewater Treatment. *Curr. Pollut. Reports* **2015**, *1*, 167–176. [CrossRef]
119. Zhang, Y.; Zhou, J.; Chen, X.; Wang, L.; Cai, W. Coupling of Heterogeneous Advanced Oxidation Processes and Photocatalysis in Efficient Degradation of Tetracycline Hydrochloride by Fe-Based MOFs: Synergistic Effect and Degradation Pathway. *Chem. Eng. J.* **2019**, *369*, 745–757. [CrossRef]
120. Garza-Campos, B.; Brillas, E.; Hernández-Ramírez, A.; El-Ghenymy, A.; Guzmán-Mar, J.L.; Ruiz-Ruiz, E.J. Salicylic Acid Degradation by Advanced Oxidation Processes. Coupling of Solar Photoelectro-Fenton and Solar Heterogeneous Photocatalysis. *J. Hazard. Mater.* **2016**, *319*, 34–42. [CrossRef]
121. Zhang, Z.; Zhang, M.; Deng, J.; Deng, K.; Zhang, B.; Lv, K.; Sun, J.; Chen, L. Potocatalytic Oxidative Degradation of Organic Pollutant with Molecular Oxygen Activated by a Novel Biomimetic Catalyst ZnPz(Dtn-COOH)$_4$. *Appl. Catal. B Environ.* **2013**, *132–133*, 90–97. [CrossRef]
122. Xie, L.; Du, T.; Wang, J.; Ma, Y.; Ni, Y.; Liu, Z.; Zhang, L.; Yang, C.; Wang, J. Recent Advances on Heterojunction-Based Photocatalysts for the Degradation of Persistent Organic Pollutants. *Chem. Eng. J.* **2021**, *426*, 130617. [CrossRef]
123. Al-Buriahi, A.K.; Al-Gheethi, A.A.; Senthil Kumar, P.; Radin Mohamed, R.M.S.; Yusof, H.; Alshalif, A.F.; Khalifa, N.A. Elimination of Rhodamine B from Textile Wastewater Using Nanoparticle Photocatalysts: A Review for Sustainable Approaches. *Chemosphere* **2022**, *287*, 132162. [CrossRef] [PubMed]
124. Tang, M.; Ao, Y.; Wang, C.; Wang, P. Facile Synthesis of Dual Z-Scheme g-C_3N_4/Ag_3PO_4/AgI Composite Photocatalysts with Enhanced Performance for the Degradation of a Typical Neonicotinoid Pesticide. *Appl. Catal. B Environ.* **2020**, *268*, 118395. [CrossRef]
125. Che, H.; Che, G.; Dong, H.; Hu, W.; Hu, H.; Liu, C.; Li, C. Fabrication of Z-Scheme Bi_3O_4Cl/g-C_3N_4 2D/2D Heterojunctions with Enhanced Interfacial Charge Separation and Photocatalytic Degradation Various Organic Pollutants Activity. *Appl. Surf. Sci.* **2018**, *455*, 705–716. [CrossRef]
126. Song, Y.; Gu, J.; Xia, K.; Yi, J.; Chen, H.; She, X.; Chen, Z.; Ding, C.; Li, H.; Xu, H. Construction of 2D SnS_2/g-C_3N_4 Z-Scheme Composite with Superior Visible-Light Photocatalytic Performance. *Appl. Surf. Sci.* **2019**, *467–468*, 56–64. [CrossRef]
127. López-Peñalver, J.J.; Sánchez-Polo, M.; Gómez-Pacheco, C.V.; Rivera-Utrilla, J. Photodegradation of Tetracyclines in Aqueous Solution by Using UV and UV/H_2O_2 Oxidation Processes. *J. Chem. Technol. Biotechnol.* **2010**, *85*, 1325–1333. [CrossRef]
128. Chen, Y.; Hu, C.; Qu, J.; Yang, M. Photodegradation of Tetracycline and Formation of Reactive Oxygen Species in Aqueous Tetracycline Solution under Simulated Sunlight Irradiation. *J. Photochem. Photobiol. A Chem.* **2008**, *197*, 81–87. [CrossRef]
129. De Godos, I.; Muñoz, R.; Guieysse, B. Tetracycline Removal during Wastewater Treatment in High-Rate Algal Ponds. *J. Hazard. Mater.* **2012**, *229–230*, 446–449. [CrossRef]
130. Kang, J.; Tang, Y.; Wang, M.; Jin, C.; Liu, J.; Li, S.; Li, Z.; Zhu, J. The Enhanced Peroxymonosulfate-Assisted Photocatalytic Degradation of Tetracycline under Visible Light by g-C_3N_4/Na-$BiVO_4$ heterojunction Catalyst and Its Mechanism. *J. Environ. Chem. Eng.* **2021**, *9*, 105524. [CrossRef]
131. Jin, C.; Wang, M.; Li, Z.; Kang, J.; Zhao, Y.; Han, J.; Wu, Z. Two Dimensional Co_3O_4/g-C_3N_4 Z-Scheme Heterojunction: Mechanism Insight into Enhanced Peroxymonosulfate-Mediated Visible Light Photocatalytic Performance. *Chem. Eng. J.* **2020**, *398*, 125569. [CrossRef]
132. Wang, S.; Teng, Z.; Xu, Y.; Yuan, M.; Zhong, Y.; Liu, S.; Wang, C.; Wang, G.; Ohno, T. Defect as the Essential Factor in Engineering Carbon-Nitride-Based Visible-Light-Driven Z-Scheme Photocatalyst. *Appl. Catal. B Environ.* **2020**, *260*, 118145. [CrossRef]
133. Aravind kumar, J.; Krithiga, T.; Sathish, S.; Renita, A.A.; Prabu, D.; Lokesh, S.; Geetha, R.; Namasivayam, S.K.R.; Sillanpaa, M. Persistent Organic Pollutants in Water Resources: Fate, Occurrence, Characterization and Risk Analysis. *Sci. Total Environ.* **2022**, *831*, 154808. [CrossRef] [PubMed]
134. Zhou, Y.; Zhou, L.; Ni, C.; He, E.; Yu, L.; Li, X. 3D/2D MOF-Derived CoCeOx/g-C_3N_4 Z-Scheme Heterojunction for Visible Light Photocatalysis: Hydrogen Production and Degradation of Carbamazepine. *J. Alloys Compd.* **2022**, *890*, 161786. [CrossRef]
135. Huang, J.; Li, D.; Li, R.; Chen, P.; Zhang, Q.; Liu, H.; Lv, W.; Liu, G.; Feng, Y. One-Step Synthesis of Phosphorus/Oxygen Co-Doped g-C_3N_4/Anatase TiO_2 Z-Scheme Photocatalyst for Significantly Enhanced Visible-Light Photocatalysis Degradation of Enrofloxacin. *J. Hazard. Mater.* **2020**, *386*, 121634. [CrossRef]
136. Meng, J.; Wang, X.; Liu, Y.; Ren, M.; Zhang, X.; Ding, X.; Guo, Y.; Yang, Y. Acid-Induced Molecule Self-Assembly Synthesis of Z-Scheme WO_3/g-C_3N_4 Heterojunctions for Robust Photocatalysis against Phenolic Pollutants. *Chem. Eng. J.* **2021**, *403*, 126354. [CrossRef]
137. Liu, N.; Lu, N.; Yu, H.T.; Chen, S.; Quan, X. Enhanced Degradation of Organic Water Pollutants by Photocatalytic In-Situ Activation of Sulfate Based on Z-Scheme g-C_3N_4/$BiPO_4$. *Chem. Eng. J.* **2022**, *428*, 132116. [CrossRef]
138. Zhang, L.; Wang, G.; Xiong, Z.; Tang, H.; Jiang, C. Fabrication of Flower-like Direct Z-Scheme β-Bi_2O_3/g-C_3N_4 Photocatalyst with Enhanced Visible Light Photoactivity for Rhodamine B Degradation. *Appl. Surf. Sci.* **2018**, *436*, 162–171. [CrossRef]
139. Li, N.; Tian, Y.; Zhao, J.; Zhang, J.; Zuo, W.; Kong, L.; Cui, H. Z-Scheme 2D/3D g-C_3N_4@ZnO with Enhanced Photocatalytic Activity for Cephalexin Oxidation under Solar Light. *Chem. Eng. J.* **2018**, *352*, 412–422. [CrossRef]
140. Qin, Y.; Li, H.; Lu, J.; Ma, C.; Liu, X.; Meng, M.; Yan, Y. Fabrication of Magnetic Quantum Dots Modified Z-Scheme Bi_2O_4/g-C_3N_4 Photocatalysts with Superior Hydroxyl Radical Productivity for the Degradation of Rhodamine B. *Appl. Surf. Sci.* **2019**, *493*, 458–469. [CrossRef]

141. Zhang, X.; Li, L.; Zeng, Y.; Liu, F.; Yuan, J.; Li, X.; Yu, Y.; Zhu, X.; Xiong, Z.; Yu, H.; et al. TiO_2/Graphitic Carbon Nitride Nanosheets for the Photocatalytic Degradation of Rhodamine B under Simulated Sunlight. *ACS Appl. Nano Mater.* **2019**, *2*, 7255–7265. [CrossRef]
142. Guo, T.; Wang, K.; Zhang, G.; Wu, X. A Novel α-Fe_2O_3@g-C_3N_4 Catalyst: Synthesis Derived from Fe-Based MOF and Its Superior Photo-Fenton Performance. *Appl. Surf. Sci.* **2019**, *469*, 331–339. [CrossRef]
143. Truc, N.T.T.; Duc, D.S.; Van Thuan, D.; Tahtamouni, T.A.; Pham, T.D.; Hanh, N.T.; Tran, D.T.; Nguyen, M.V.; Dang, N.M.; Le Chi, N.T.P.; et al. The Advanced Photocatalytic Degradation of Atrazine by Direct Z-Scheme Cu Doped ZnO/g-C_3N_4. *Appl. Surf. Sci.* **2019**, *489*, 875–882. [CrossRef]
144. Gayathri, K.; Teja, Y.N.; Prakash, R.M.; Hossain, M.S.; Alsalme, A.; Sundaravadivel, E.; Sakar, M. In Situ-Grown ZnO Particles on g-C_3N_4 Layers: A Direct Z-Scheme-Driven Photocatalyst for the Degradation of Dye and Pharmaceutical Pollutants under Solar Irradiation. *J. Mater. Sci. Mater. Electron.* **2022**, *33*, 9774–9784. [CrossRef]
145. Jain, I.P. Hydrogen the Fuel for 21st Century. *Int. J. Hydrogen Energy* **2009**, *34*, 7368–7378. [CrossRef]
146. Nazir, H.; Louis, C.; Jose, S.; Prakash, J.; Muthuswamy, N.; Buan, M.E.M.; Flox, C.; Chavan, S.; Shi, X.; Kauranen, P.; et al. Is the H_2 Economy Realizable in the Foreseeable Future? Part I: H_2 Production Methods. *Int. J. Hydrogen Energy* **2020**, *45*, 13777–13788. [CrossRef]
147. Jafari, T.; Moharreri, E.; Amin, A.S.; Miao, R.; Song, W.; Suib, S.L. Photocatalytic Water Splitting-The Untamed Dream: A Review of Recent Advances. *Molecules* **2016**, *21*, 900. [CrossRef]
148. Fajrina, N.; Tahir, M. A Critical Review in Strategies to Improve Photocatalytic Water Splitting towards Hydrogen Production. *Int. J. Hydrogen Energy* **2019**, *44*, 540–577. [CrossRef]
149. Wang, Q.; Domen, K. Particulate Photocatalysts for Light-Driven Water Splitting: Mechanisms, Challenges, and Design Strategies. *Chem. Rev.* **2020**, *120*, 919–985. [CrossRef]
150. Chen, X.; Shi, R.; Chen, Q.; Zhang, Z.; Jiang, W.; Zhu, Y.; Zhang, T. Three-Dimensional Porous g-C_3N_4 for Highly Efficient Photocatalytic Overall Water Splitting. *Nano Energy* **2019**, *59*, 644–650. [CrossRef]
151. Ye, R.; Fang, H.; Zheng, Y.Z.; Li, N.; Wang, Y.; Tao, X. Fabrication of $CoTiO_3$/g-C_3N_4 Hybrid Photocatalysts with Enhanced H_2 Evolution: Z-Scheme Photocatalytic Mechanism Insight. *ACS Appl. Mater. Interfaces* **2016**, *8*, 13879–13889. [CrossRef] [PubMed]
152. She, X.; Wu, J.; Xu, H.; Zhong, J.; Wang, Y.; Song, Y.; Nie, K.; Liu, Y.; Yang, Y.; Rodrigues, M.T.F.; et al. High Efficiency Photocatalytic Water Splitting Using 2D A-Fe_2O_3/g-C_3N_4 Z-Scheme Catalysts. *Adv. Energy Mater.* **2017**, *7*, 1700025. [CrossRef]
153. Yang, Y.; Qiu, M.; Li, L.; Pi, Y.; Yan, G.; Yang, L. A Direct Z-Scheme Van Der Waals Heterojunction ($WO_3 \cdot H_2O$/g-C_3N_4) for High Efficient Overall Water Splitting under Visible-Light. *Sol. RRL* **2018**, *2*, 1800148. [CrossRef]
154. Kong, L.; Zhang, X.; Wang, C.; Xu, J.; Du, X.; Li, L. Ti^{3+} Defect Mediated G-C_3N_4 /TiO_2 Z-Scheme System for Enhanced Photocatalytic Redox Performance. *Appl. Surf. Sci.* **2018**, *448*, 288–296. [CrossRef]
155. Qin, S.; Lei, Y.; Guo, J.; Huang, J.F.; Hou, C.P.; Liu, J.M. Constructing Heterogeneous Direct Z-Scheme Photocatalysts Based on Metal-Organic Cages and Graphitic-C_3N_4 for High-Efficiency Photocatalytic Water Splitting. *ACS Appl. Mater. Interfaces* **2021**, *13*, 25960–25971. [CrossRef]
156. Wang, J.; Xia, Y.; Zhao, H.; Wang, G.; Xiang, L.; Xu, J.; Komarneni, S. Oxygen Defects-Mediated Z-Scheme Charge Separation in g-C_3N_4/ZnO Photocatalysts for Enhanced Visible-Light Degradation of 4-Chlorophenol and Hydrogen Evolution. *Appl. Catal. B Environ.* **2017**, *206*, 406–416. [CrossRef]
157. Shi, Y.; Chen, J.; Mao, Z.; Fahlman, B.D.; Wang, D. Construction of Z-Scheme Heterostructure with Enhanced Photocatalytic H_2 Evolution for g-C_3N_4 Nanosheets via Loading Porous Silicon. *J. Catal.* **2017**, *356*, 22–31. [CrossRef]
158. Yang, C.; Xue, Z.; Qin, J.; Sawangphruk, M.; Rajendran, S.; Zhang, X.; Liu, R. Visible Light-Driven Photocatalytic H_2 Generation and Mechanism Insights into $Bi_2O_2CO_3$ /G-C_3N_4 Z-Scheme Photocatalyst. *J. Phys. Chem. C* **2019**, *123*, 4795–4804. [CrossRef]
159. Cui, Y.; Wang, H.; Yang, C.; Li, M.; Zhao, Y.; Chen, F. Post-Activation of in Situ B–F Codoped g-C_3N_4 for Enhanced Photocatalytic H_2 Evolution. *Appl. Surf. Sci.* **2018**, *441*, 621–630. [CrossRef]
160. Xu, B.; Wang, B.; Zhang, H.; Yang, P. Z-Scheme Cu_2O Nanoparticle/Graphite Carbon Nitride Nanosheet Heterojunctions for Photocatalytic Hydrogen Evolution. *ACS Appl. Nano Mater.* **2022**, *5*, 8475–8483. [CrossRef]
161. Olabi, A.G.; Abdelkareem, M.A. Renewable Energy and Climate Change. *Renew. Sustain. Energy Rev.* **2022**, *158*, 112111. [CrossRef]
162. Kuc, T.; Rozanski, K.; Zimnoch, M.; Necki, J.M.; Korus, A. Anthropogenic Emissions of CO_2 and CH_4 in an Urban Environment. *Appl. Energy* **2003**, *75*, 193–203. [CrossRef]
163. Sullivan, I.; Goryachev, A.; Digdaya, I.A.; Li, X.; Atwater, H.A.; Vermaas, D.A.; Xiang, C. Coupling Electrochemical CO_2 Conversion with CO_2 Capture. *Nat. Catal.* **2021**, *4*, 952–958. [CrossRef]
164. Lewis, N.S. Developing a Scalable Artificial Photosynthesis Technology through Nanomaterials by Design. *Nat. Nanotechnol.* **2016**, *11*, 1010–1019. [CrossRef] [PubMed]
165. Greenwood, N.N.; Earnshaw, A. *Chemistry of the Elements*, 2nd ed.; Elsevier Butterworth-Heinemann: Oxford, UK, 2005.
166. Khalil, M.; Gunlazuardi, J.; Ivandini, T.A.; Umar, A. Photocatalytic Conversion of CO_2 Using Earth-Abundant Catalysts: A Review on Mechanism and Catalytic Performance. *Renew. Sustain. Energy Rev.* **2019**, *113*, 109246. [CrossRef]
167. Chang, X.; Wang, T.; Gong, J. CO_2 Photo-Reduction: Insights into CO_2 Activation and Reaction on Surfaces of Photocatalysts. *Energy Environ. Sci.* **2016**, *9*, 2177–2196. [CrossRef]
168. Collado, L.; Reynal, A.; Coronado, J.M.; Serrano, D.P.; Durrant, J.R.; De la Peña O'Shea, V.A. Effect of Au Surface Plasmon Nanoparticles on the Selective CO_2 Photoreduction to CH_4. *Appl. Catal. B Environ.* **2015**, *178*, 177–185. [CrossRef]

169. Dong, G.; Zhang, L. Porous Structure Dependent Photoreactivity of Graphitic Carbon Nitride under Visible Light. *J. Mater. Chem.* **2012**, *22*, 1160–1166. [CrossRef]
170. Jiang, Z.; Wan, W.; Li, H.; Yuan, S.; Zhao, H.; Wong, P.K. A Hierarchical Z-Scheme α-Fe_2O_3/g-C_3N_4 Hybrid for Enhanced Photocatalytic CO_2 Reduction. *Adv. Mater.* **2018**, *30*, 1706108. [CrossRef]
171. Liu, T.; Hao, L.; Bai, L.; Liu, J.; Zhang, Y.; Tian, N.; Huang, H. Z-Scheme Junction $Bi_2O_2(NO_3)(OH)$/g-C_3N_4 for Promoting CO_2 Photoreduction. *Chem. Eng. J.* **2022**, *429*, 132268. [CrossRef]
172. Yu, W.; Xu, D.; Peng, T. Enhanced Photocatalytic Activity of G-C_3N_4 for Selective CO_2 Reduction to CH_3OH via Facile Coupling of ZnO: A Direct Z-Scheme Mechanism. *J. Mater. Chem. A* **2015**, *3*, 19936–19947. [CrossRef]
173. Thanh Truc, N.T.; Giang Bach, L.; Thi Hanh, N.; Pham, T.D.; Thi Phuong Le Chi, N.; Tran, D.T.; Nguyen, M.V.; Nguyen, V.N. The Superior Photocatalytic Activity of Nb Doped TiO_2/g-C_3N_4 Direct Z-Scheme System for Efficient Conversion of CO_2 into Valuable Fuels. *J. Colloid Interface Sci.* **2019**, *540*, 1–8. [CrossRef] [PubMed]
174. Zhao, J.; Ji, M.; Chen, H.; Weng, Y.X.; Zhong, J.; Li, Y.; Wang, S.; Chen, Z.; Xia, J.; Li, H. Interfacial Chemical Bond Modulated $Bi_{19}S_{27}Br_3$/g-C_3N_4 Z-Scheme Heterojunction for Enhanced Photocatalytic CO_2 Conversion. *Appl. Catal. B Environ.* **2022**, *307*, 121162. [CrossRef]
175. Murugesan, P.; Narayanan, S.; Manickam, M.; Murugesan, P.K.; Subbiah, R. A Direct Z-Scheme Plasmonic AgCl@g-C_3N_4 Heterojunction Photocatalyst with Superior Visible Light CO_2 Reduction in Aqueous Medium. *Appl. Surf. Sci.* **2018**, *450*, 516–526. [CrossRef]
176. Thanh Truc, N.T.; Hanh, N.T.; Nguyen, M.V.; Le Chi, N.T.P.; Van Noi, N.; Tran, D.T.; Ha, M.N.; Trung, D.Q.; Pham, T.D. Novel Direct Z-Scheme $Cu_2V_2O_7$/g-C_3N_4 for Visible Light Photocatalytic Conversion of CO_2 into Valuable Fuels. *Appl. Surf. Sci.* **2018**, *457*, 968–974. [CrossRef]
177. Thanh Truc, N.T.; Pham, T.D.; Nguyen, M.V.; Van Thuan, D.; Trung, D.Q.; Thao, P.; Trang, H.T.; Nguyen, V.N.; Tran, D.T.; Minh, D.N.; et al. Advanced $NiMoO_4$/g-C_3N_4 Z-Scheme Heterojunction Photocatalyst for Efficient Conversion of CO_2 to Valuable Products. *J. Alloys Compd.* **2020**, *842*, 155860. [CrossRef]
178. Shen, Y.; Han, Q.; Hu, J.; Gao, W.; Wang, L.; Yang, L.; Gao, C.; Shen, Q.; Wu, C.; Wang, X.; et al. Artificial Trees for Artificial Photosynthesis: Construction of Dendrite-Structured α-Fe_2O_3/g-C_3N_4Z-Scheme System for Efficient CO_2 Reduction into Solar Fuels. *ACS Appl. Energy Mater.* **2020**, *3*, 6561–6572. [CrossRef]
179. Wang, K.; Jiang, L.; Wu, X.; Zhang, G. Vacancy Mediated Z-Scheme Charge Transfer in a 2D/2D $La_2Ti_2O_7$/g-C_3N_4 nanojunction as a Bifunctional Photocatalyst for Solar-to-Energy Conversion. *J. Mater. Chem. A* **2020**, *8*, 13241–13247. [CrossRef]
180. Guo, R.T.; Liu, X.Y.; Qin, H.; Wang, Z.Y.; Shi, X.; Pan, W.G.; Fu, Z.G.; Tang, J.Y.; Jia, P.Y.; Miao, Y.F.; et al. Photocatalytic Reduction of CO_2 into CO over Nanostructure Bi_2S_3 Quantum Dots/g-C_3N_4 Composites with Z-Scheme Mechanism. *Appl. Surf. Sci.* **2020**, *500*, 144059. [CrossRef]
181. Zhu, L.; Li, H.; Xu, Q.; Xiong, D.; Xia, P. High-Efficient Separation of Photoinduced Carriers on Double Z-Scheme Heterojunction for Superior Photocatalytic CO_2 Reduction. *J. Colloid Interface Sci.* **2020**, *564*, 303–312. [CrossRef]
182. Guo, H.; Wan, S.; Wang, Y.; Ma, W.; Zhong, Q.; Ding, J. Enhanced Photocatalytic CO_2 Reduction over Direct Z-Scheme $NiTiO_3$/g-C_3N_4 Nanocomposite Promoted by Efficient Interfacial Charge Transfer. *Chem. Eng. J.* **2021**, *412*, 128646. [CrossRef]